OAK RIDGE NATIONAL LABORATORY

MANAGED BY UT-BATTELLE FOR THE DEPARTMENT OF ENERGY

ORNL/SUB/00-XSZ175V-2

Neutronic Benchmarks for the Utilization of Mixed-Oxide Fuel: Joint U.S./Russian Progress Report for Fiscal Year 1997

Volume 4, Part 2—Saxton Plutonium Program Critical Experiments

Naeem M. Abdurrahman
Igor Carron
Georgeta Radulescu

Fissile Materials Disposition Program

UT-BATTELLE

ORNL-27 (4-00)

ORNL/SUB/00-XSZ175V-2

Neutronic Benchmarks for the Utilization of Mixed-Oxide Fuel: Joint U.S./Russian Progress Report for Fiscal Year 1997

Volume 4, Part 2—Saxton Plutonium Program Critical Experiments

Naeem M. Abdurrahman
The University of Texas at Austin

Igor Carron
Texas A&M University

Georgeta Radulescu
The University of Texas at Austin

Date Published: September 2000

Prepared by the
OAK RIDGE NATIONAL LABORATORY
Oak Ridge, Tennessee 37831
managed by
UT-BATTELLE, LLC
for the
U.S. DEPARTMENT OF ENERGY
under contract DE-AC05-00OR22725

CONTENTS

LIST OF TABLES

LIST OF FIGURES

Figure **Page**

1. DETAILED DESCRIPTION

1.1 OVERVIEW OF EXPERIMENT

Critical experiments with water-moderated, single-region PuO_2-UO_2 or UO_2, and multiple-region PuO_2-UO_2- and UO_2-fueled cores were performed at the CRX reactor critical facility at the Westinghouse Reactor Evaluation Center (WREC) at Waltz Mill, Pennsylvania in 1965 [1]. These critical experiments were part of the Saxton Plutonium Program. The mixed oxide (MOX) fuel used in these critical experiments and then loaded in the Saxton reactor contained 6.6 wt% PuO_2 in a mixture of PuO_2 and natural UO_2. The Pu metal had the following isotopic mass percentages: 90.50% ^{239}Pu; 8.57% ^{239}Pu; 0.89% ^{240}Pu; and 0.04% ^{241}Pu. The purpose of these critical experiments was to verify the nuclear design of Saxton partial plutonium cores while obtaining parameters of fundamental significance such as buckling, control rod worth, soluble poison worth, flux, power peaking, relative pin power, and power sharing factors of MOX and UO_2 lattices. For comparison purposes, the core was also loaded with uranium dioxide fuel rods only. This series is covered by experiments beginning with the designation SX.

1.2 DESCRIPTION OF EXPERIMENTAL CONFIGURATION

The CRX reactor was a critical facility designed to be controlled by partial moderator level adjustments. The experiments were performed inside a large aluminum tank containing water, as shown in Fig. 1. The height of the moderator could be adjusted in order to render the configuration critical. The nuclear instrumentation included boron trifluoride detectors for the start-up range and seven ion chambers for the operating range. Three major types of experimentation were performed: single-region, multiregion, and void-effect experiments.

In the single-region experiments, only one type of fuel, MOX or UO_2, was present in the lattice. The single-region critical core configurations included fuel patterns with five different lattice pitches: 1.3208, 1.4224, 1.8679, 2.0016, and 2.6416 cm (0.52, 0.56, 0.73539, 0.79196, and 1.04 in.) for buckling and reflector saving measurements. MOX or UO_2 fuel cores, with a 1.4224-cm (0.56-in.) lattice pitch, perturbed by a water slot, an aluminum plate, and control rods were used for measurements of relative power distributions and reactivity worth of perturbations to uniform critical lattices. The reactivity worth of boron at different concentrations was also measured for MOX fuel cores. The UO_2 lattices were included in this presentation for comparison purposes, since uranium lattice parameters are more accurately known.

The second type of experimentation included multiregion experiments, where a lattice composed of one of the two fuels was surrounded by a lattice of the other fuel. These experiments were performed on lattices with the pitch of 1.4224 cm (0.56 in.) in order to evaluate the relative pin power distributions.

Voiding-effect experiments were performed on 1.3208-cm (0.52 in.) pitch MOX single-region and multiregion cores with various void tube patterns.

Dimensions for the various core components are given in the following sections in preferred unit. The number of digits cited for values converted from English to metric units does not indicate the accuracy; it is an artifact of the conversion process. To clarify Fig. 1, the core tank thickness was 5.08 cm (2 inches). The distance from the bottom of the core tank to the floor was 10.16 cm (4 inches).

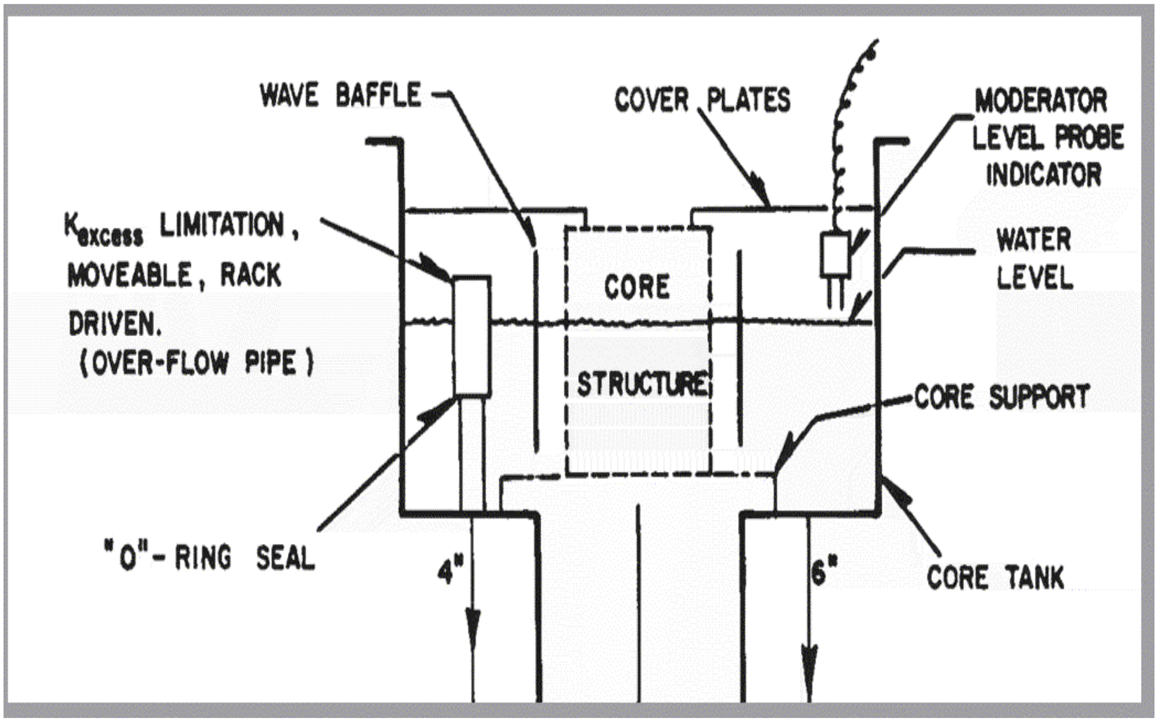

Figure 1. CRX moderator system.

1.2.1 Description of the Lattice

The general lattice assembly is provided in Fig. 2.

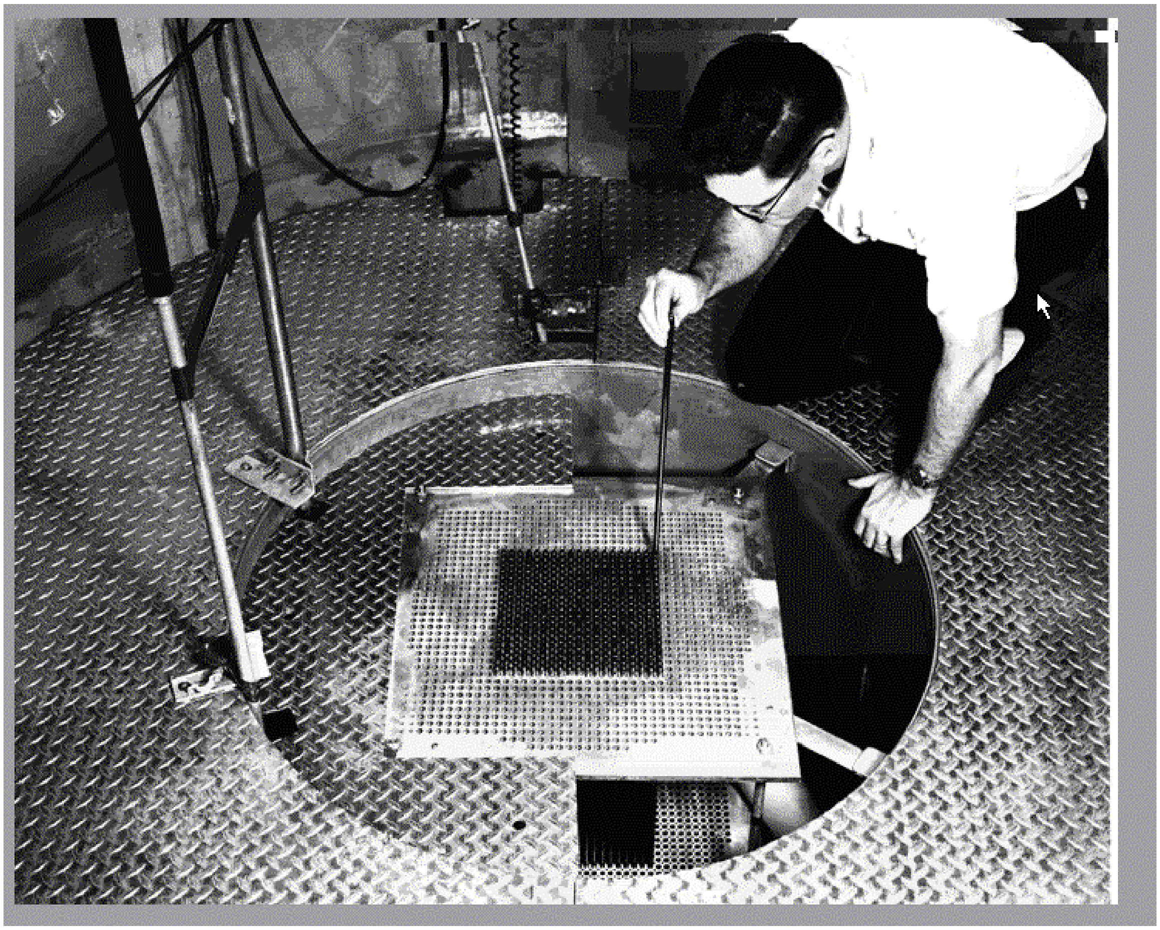

Figure 2. Top view of the WREC-CRX core.

Five lattice pitches were used in the Saxton critical experiments: 1.3208 cm (0.52 in.); 1.4224 cm (0.56 in.); 1.86789 cm (0.73539 in.); 2.01158 cm (0.79196 in.); and 2.6416 cm (1.04 in.). The lattice pitch of the guiding plates was different in only two cases 1.3208 cm (0.52 in.) and 1.4224 cm (0.56 in.). Two additional pitches were obtained by loading fuel rods on core diagonals at lattice pitches that were $\sqrt{2}$ times the original pitches. The fifth pitch was obtained by placing fuel rods every other hole in the 1.3208-cm (0.52-in.) lattice, leading to a 2.6416-cm (1.04-in.) lattice pitch. A typical original 19×19 lattice square configuration is shown in Fig. 3.

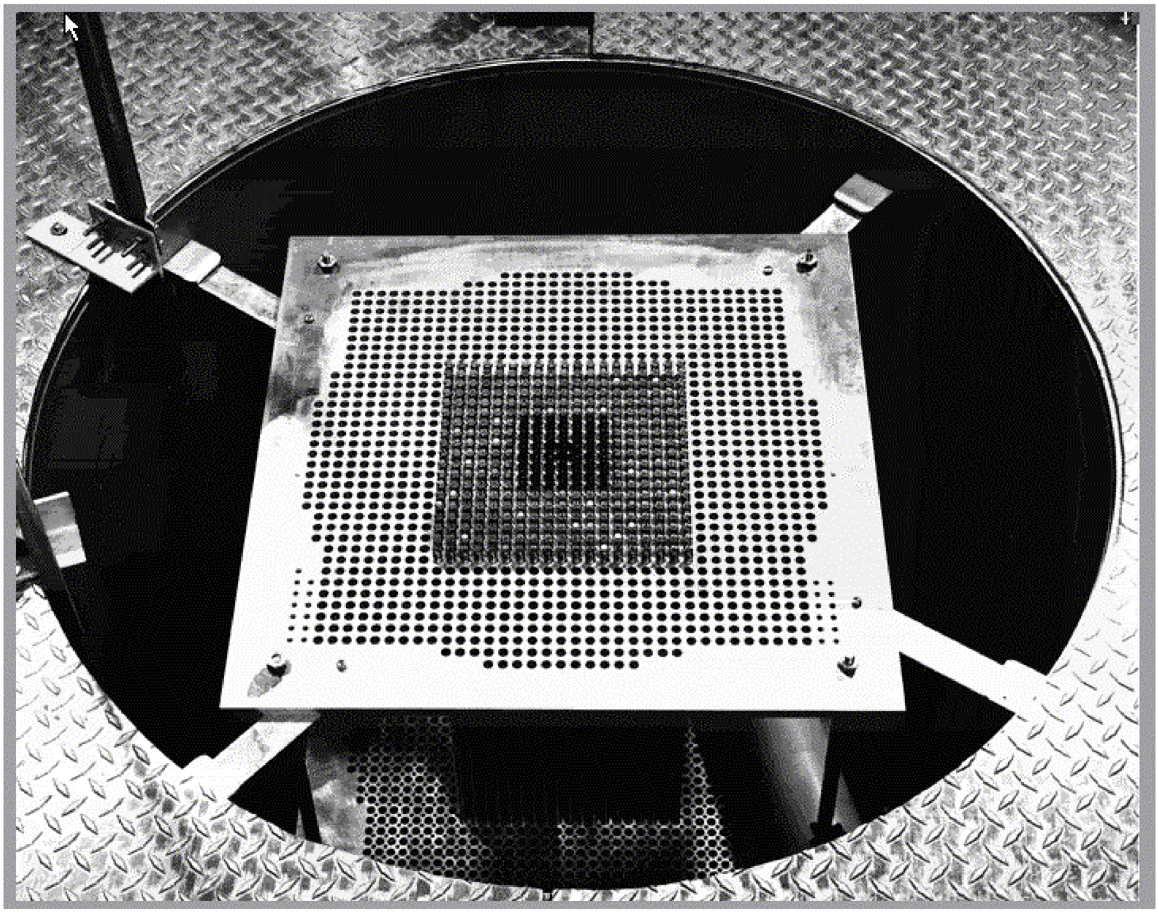

Figure 3. 7×7 MOX insert in a 19×19 UO_2 loading.

Table 1.1 is a summary of the critical, partially inundated, cores used for various experiments. The fully reflected just critical cores were not included in this table, because the core configurations were not provided in Ref. 1. Also, three other partially inundated critical cores were not included in this table. One critical core (Configuration 7 of the relative power experiments) had several Vipac MOX fuel rods among pelletized MOX fuel rods. Two multiregion critical cores of the void-effect experiments were not included because of an inconsistency regarding the description of the void tube pitch in a table (Table I, App. 2, p. 2, Ref. 1) and figures (Figures 16 and 17, App. E, pp. 20 and 21, respectively, Ref. 1). The different categories of the table are explained thereafter.

Table 1.1. Summary of the Saxton critical experiments

Case	Designation[1]	Core shape[2]	Lattice pitch (cm)	Water Temperature (^{0}C)	Critical water height[3] (cm)	Boron concentration (ppm)	Inner region fuel and size[4]	Outer region fuel	Core size	Experiment type[5]
1	SX1.2.1	S	1.4224	17.0	82.46	0	MOX 19×19	N/A	N/A	buckling
2	SX1.2.2	S	1.4224	15.75	83.45	0	MOX 19×19	N/A	N/A	buckling relative power
3	SX1.2.3	s (see Sect. 1.2.5)	1.4224	15.4	75.90	0	MOX 19×19 water slot at center	N/A	N/A	relative power reactivity worth
4	SX1.2.4	s (see Sect. 1.2.5)	1.4224	16.0	83.02	0	MOX 19×19 Al slab at center	N/A	N/A	relative power reactivity worth
5	SX1.2.5	s (see Sect. 1.2.5)	1.4224	15.4	79.01	0	MOX 21×21 5 control rods at center	N/A	N/A	relative power reactivity worth
6	SX1.2.6	S	1.4224	17.0	82.41	0	MOX 19×19	N/A	N/A	reactivity worth
7	SX1.2.7	S	1.4224	16.9	89.41	25	MOX 19×19	N/A	N/A	reactivity worth
8	SX1.2.8	S	1.4224	16.9	99.44	50	MOX 19×19	N/A	N/A	reactivity worth
9	SX1.2.9	S	1.4224	15.4	52.13	0	MOX 21×21	N/A	N/A	reactivity worth
10	SX1.2.10	S	1.4224	18.0	72.47	228	MOX 21×21	N/A	N/A	reactivity worth
11	SX1.2.11	S	1.4224	18.0	84.66	309	MOX 21×21	N/A	N/A	reactivity worth
12	SX1.2.12	S	1.4224	18.0	89.70	337	MOX 21×21	N/A	N/A	reactivity worth buckling
13	SX1.4.1	s (Fig. 5)	2.01158	16.1	78.43	0	MOX 12×12	N/A	N/A	buckling
14	SX1.1.1	R	1.3208	25.8	84.56	0	MOX 22×23	N/A	N/A	buckling
15	SX1.3.1	s (Fig. 6)	1.86789	24.1	70.11	0	MOX 13×13	N/A	N/A	buckling
16	SX1.5.1	S	2.6416	19.9	81.17	0	MOX 11×11	N/A	N/A	buckling
17	SX2.2.1	S	1.4224	18.0	83.71	0	UO_2 19×19	N/A	N/A	buckling
18	SX2.2.2	S	1.4224	18.4	83.60	0	UO_2 19×19	N/A	N/A	reactivity worth

[1] SX refers to the present critical series. The next number corresponds to the type of fuel composing the cores: 1 refers to MOX cores; 2 refers to UO_2 cores; 3 and 4 refer to multiregion cores with MOX fuel in the inner region and UO_2 fuel in the outer region, clean and borated, respectively; 5 and 6 refer to multiregion cores with UO_2 fuel in the inner region and MOX fuel in the outer region clean and borated, respectively. The next number corresponds to the lattice pitch size (1, 2, 3, 4, and 5 refer to 1.3208-cm (0.52-in.), 1.4224-cm (0.56-in.), 1.8679-cm (0.73539-in.), 2.0116-cm (0.79196-in.), and 2.6416-cm (1.04-in.) pitches, respectively). The last number is an order number within each cathegory defined by the first two numbers.

[2] "c", "s", and "r" mean a cylindrical configuration, a square configuration, and a rectangular configuration, respectively. Some loading patterns are shown in Figures 4 through 23.

[3] Critical water height for each core configuration is H_{corr}=0.997(H_{raw}+1.91) cm, where H_{raw} is the critical water height reported in Ref. 1.

[4] For single-region configurations, "size" refers to core size.

[5] The type of measurements performed for each case.

Case	Designation[1]	Core shape[2]	Lattice pitch (cm)	Water Temperature (^{0}C)	Critical water height[3] (cm)	Boron concentration (ppm)	Inner region fuel and size[4]	Outer region fuel	Core size	Experiment type[5]
19	SX2.2.3	s (see Sect. 1.2.5)	1.4224	18.4	80.00	0	UO_2 19×19 water slot at center	N/A	N/A	reactivity worth
20	SX2.2.4	s (see Sect. 1.2.5)	1.4224	18.0	87.38	0	UO_2 19×19 Al slab at center	N/A	N/A	reactivity worth
21	SX2.2.5	s	1.4224	16.1	52.75	0	UO_2 21×21	N/A	N/A	reactivity worth
22	SX2.2.6	s (see Sect. 1.2.5)	1.4224	18.0	89.02	0	UO_2 21×21 5 control rods at center	N/A	N/A	relative power reactivity worth
23	SX2.4.1	r (Fig. 4)	2.01158	17.3	90.60	0	UO_2 13×14	N/A	N/A	buckling
24	SX2.1.1	c (Fig. 12)	1.3208	19.2	95.25	0	UO_2 449	N/A	N/A	buckling
25	SX3.2.1	S	1.4224	21.2	83.83	0	MOX 3×3	UO_2	19×19	relative power
26	SX3.2.2	S	1.4224	16.2	91.07	0	MOX 11×11	UO_2	19×19	relative power
27	SX3.2.3	s (Fig. 8)	1.4224	15.0	92.07	0	MOX 11×11 Al slab at fuel interface	UO_2	19×19	relative power
28	SX3.2.4	s (Fig. 9)	1.4224	15.5	73.55	0	MOX 11×11 5 control rods at fuel interface	UO_2	21×21	relative power
29	SX4.2.1	S	1.4224	18.2	93.35	1,453	MOX 19×19	UO_2	27×27	relative power
30	SX4.2.2	S	1.4224	18.5	89.14	1,425	MOX 19×19 3x3 UO_2 insert at center	UO_2	27×27	relative power
31	SX4.2.3	s (Fig. 7)	1.4224	18.5	92.19	1,425	MOX 19×19 L-shaped UO_2 insert	UO_2	27×27	relative power
32	SX4.2.4	s (Fig. 10)	1.4224	18.0	99.80	1,453	MOX 19×19 water slot at fuel interface	UO_2	27×27	relative power
33	SX4.2.5	s (Fig. 11)	1.4224	17.8	106.35	1,453	MOX 19×19 Al plate at fuel interface	UO_2	27×27	relative power
34	SX5.2.1	S	1.4224	15.6	76.11	0	UO_2 11×11	MOX	19×19	relative power
35	SX6.2.1	s	1.4224	20	86.70	1,252	UO_2 19×19	MOX	27×27	relative power
36	SX1.1.2	s	1.3208	19.5	76.01	0	MOX 23×23	N/A	N/A	void-effects
37	SX1.1.3	s (Fig. 13)	1.3208	19.5	96.67	0	MOX 23×23, 8x8 void tubes	N/A	N/A	void-effects
38	SX1.1.4	r (Fig. 14)	1.3208	18.9	74.78	0	MOX 25×23, 8x8 void tubes	N/A	N/A	void-effects
39	SX1.1.5	r (Fig. 15)	1.3208	18.9	93.89	0	MOX 25×23, 12x12 void tubes	N/A	N/A	void-effects
40	SX1.1.6	r (Fig.16)	1.3208	19.8	75.44	0	MOX 25×23, 72 void tubes	N/A	N/A	void-effects
41	SX1.1.7	r (Fig. 19)	1.3208	19.0	94.98	0	MOX 25×24, 276 void tubes	N/A	N/A	void-effects
42	SX1.1.8	r (Fig. 17)	1.3208	18.9	78.91	0	MOX 25×24, 153 void tubes	N/A	N/A	void-effects
43	SX1.1.9	r (Fig. 18)	1.3208	18.9	70.66	0	MOX 25×24, 91 void tubes	N/A	N/A	void-effects

Case	Designation[1]	Core shape[2]	Lattice pitch (cm)	Water Temperature (^{0}C)	Critical water height[3] (cm)	Boron concentration (ppm)	Inner region fuel and size[4]	Outer region fuel	Core size	Experiment type[5]
44	SX1.1.10	r	1.3208	18.9	58.95	0	MOX 25×24	N/A	N/A	void-effects
45	SX1.1.11	s	1.3208	19.6	75.66	0	MOX 23×23	N/A	N/A	void-effects
46	SX1.1.12	s (Fig. 22)	1.3208	19.5	79.83	0	MOX 23×23, 4x4 void tubes	N/A	N/A	void-effects
47	SX1.1.13	s (Fig. 23)	1.3208	19.6	79.55	0	MOX 23×23, 4x4 void tubes	N/A	N/A	void-effects
48	SX1.1.14	s (Fig. 20)	1.3208	19.9	78.87	0	MOX 23×23, 4x4 void tubes	N/A	N/A	void-effects
49	SX1.1.15	s (Fig. 21)	1.3208	19.8	77.95	0	MOX 23×23, 4x4 void tubes	N/A	N/A	void-effects

1.2.2 Special Loading Patterns

The fuel patterns for some critical configurations--including lattices with pitches greater than 1.4224 cm (0.56 in.), a cylindrical core configuration, perturbed multiregion arrangements through a water slot, an aluminum slab, and five control rods, and void-effect configurations--are shown in this section. The fuel rods are located at the center of each square of the lattices displayed in Figures 4 through 12 and the fuel load is also suggested in these figures. For the cores of the void-effect experiments, presented in Figures 13 through 23, only the void tube arrangement is shown and the fuel rods are located at the intersection of the table grids. In every figure, the bold lines represent the limit of a loading pattern for a fuel region. The "x" in each figure represents the center pin in the array.

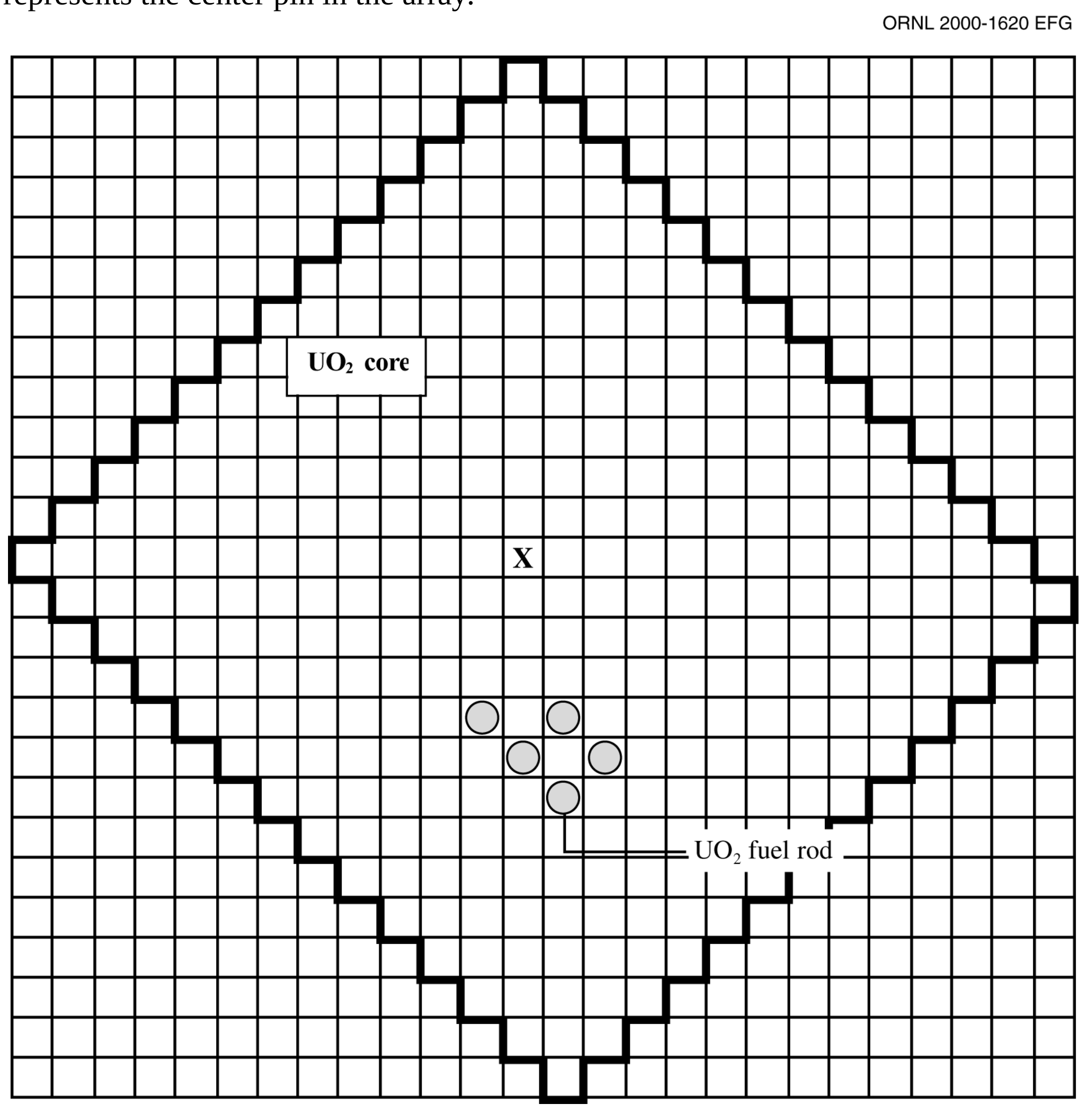

Figure 4. SX2.4.1: UO_2 13x14 rectangle core and 2.0116-cm (0.79196-in.) lattice pitch[6].

[6] Fig. B-1, p. 47, Ref. 1.

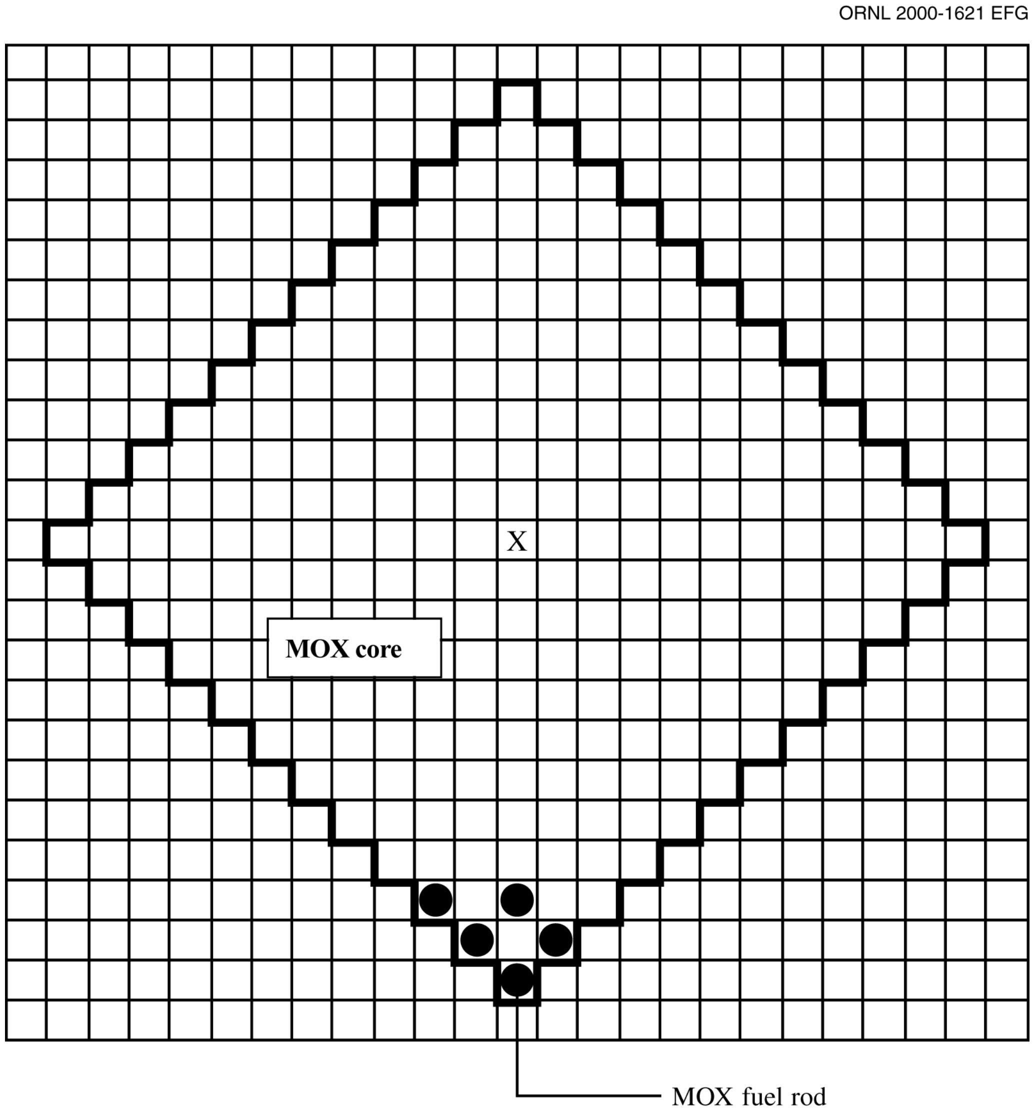

Figure 5. SX1.4.1: MOX 12x12 square core and 2.0116-cm (0.79196-in.) lattice pitch[7].

[7] Fig. B-3, p. 56, Ref. 1.

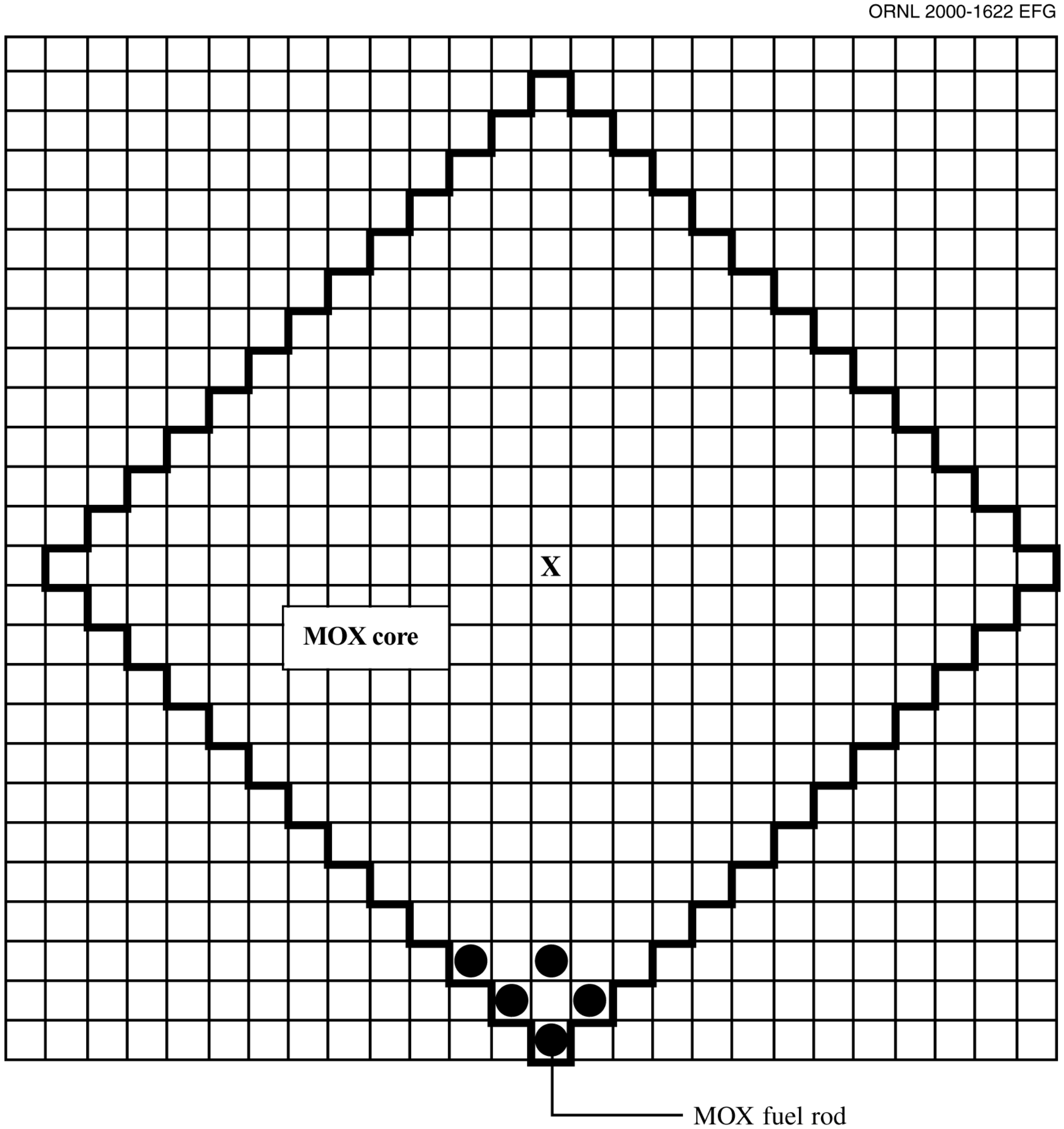

Figure 6. SX1.3.1: MOX 13x13 square core and 1.8679-cm (0.73539-in.) lattice pitch[8].

[8] Fig. B-6, p. 69, Ref. 1.

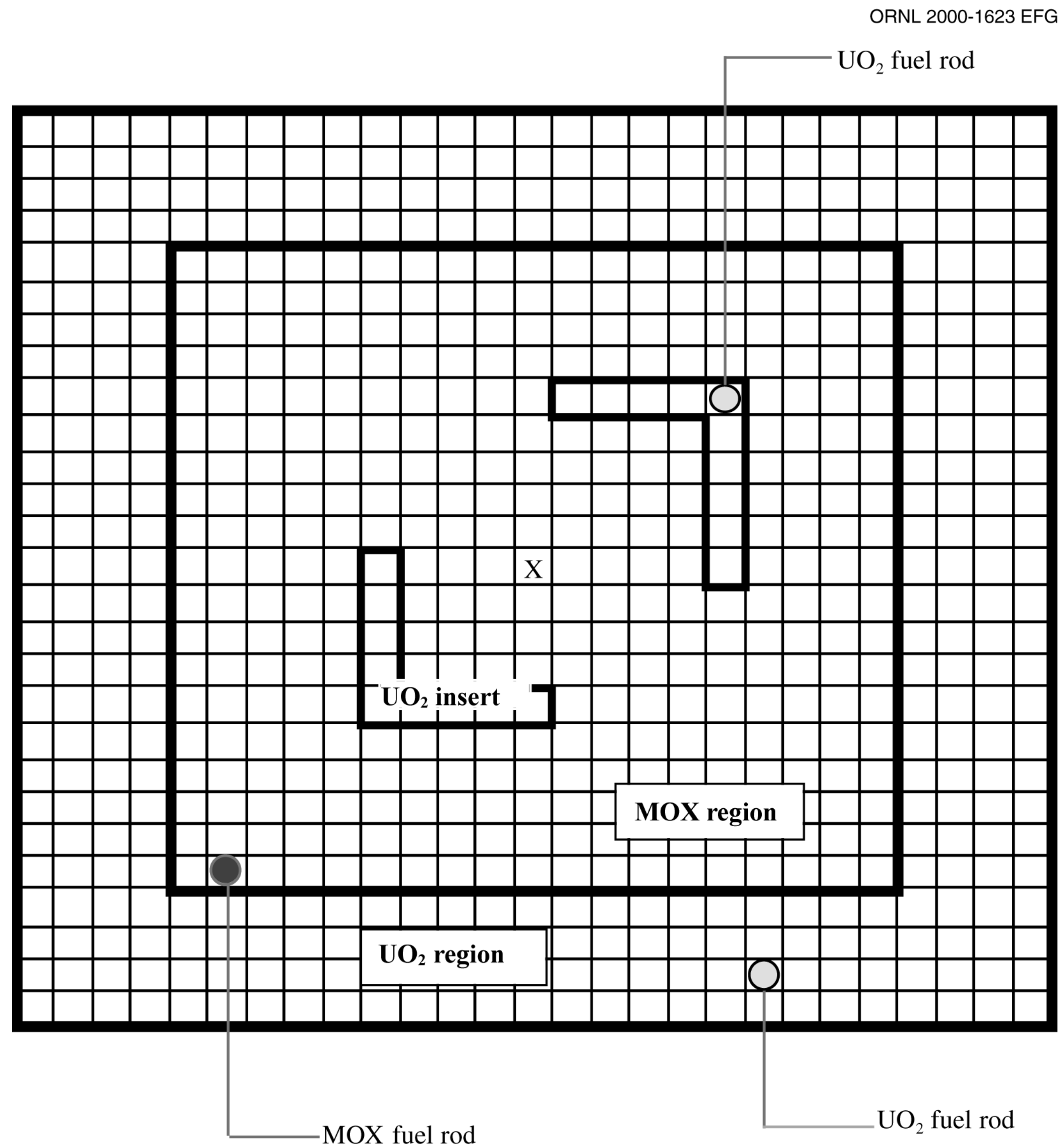

Figure 7. SX4.2.3: 27x27 core, 19x19 MOX inner region, L shaped insert and outer region UO_2, and 1.4224-cm (0.56-in.) lattice pitch[9].

[9] Fig. p. 44, A-8, Att. A, Ref. 1.

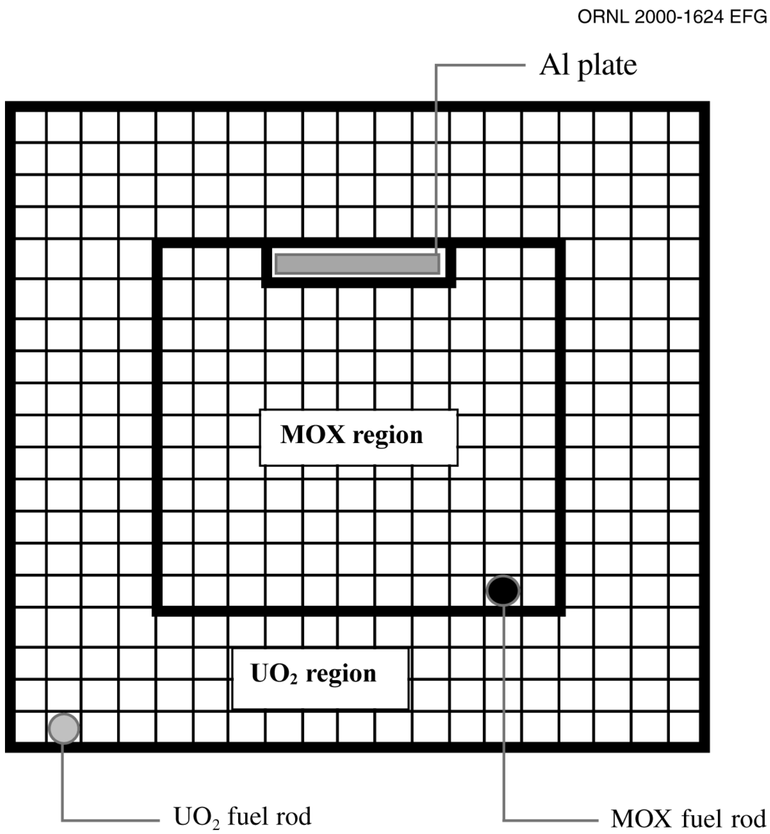

Figure 8. SX3.2.3: 19x19 core, 11x11 MOX center region, UO_2 outer region, aluminum slab at region boundary, and 1.4224-cm (0.56-in.) lattice pitch[10].

[10] Fig. A-9, p. 45, Att. A, Ref. 1.

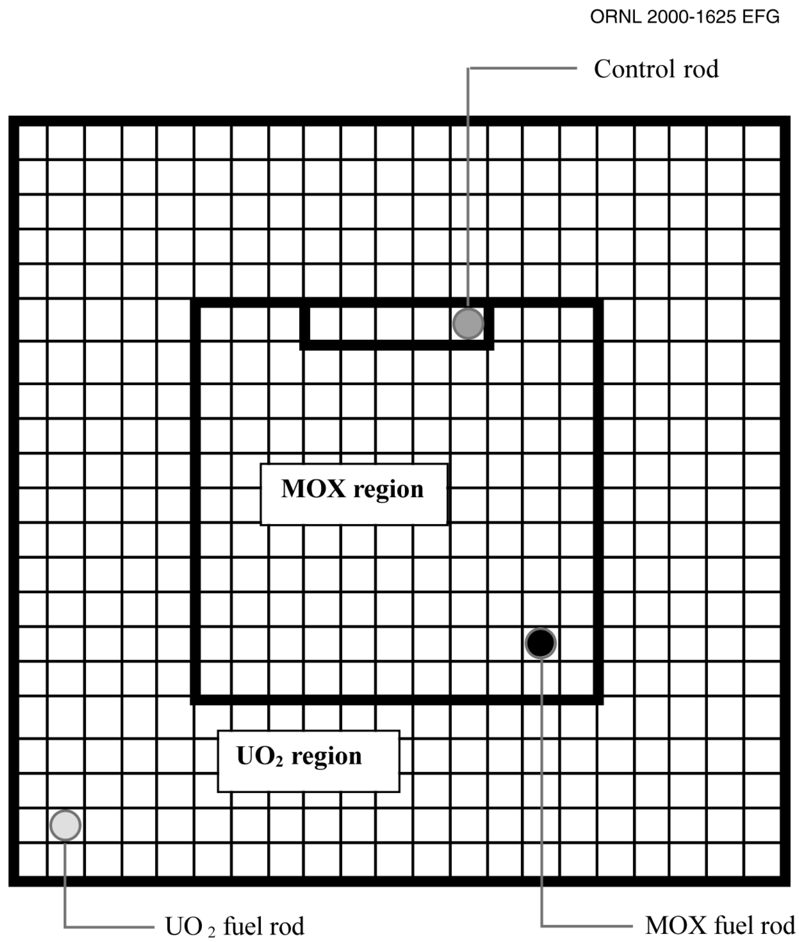

Figure 9. SX3.2.4: 21x21 core, 11x11 MOX center region, UO_2 outer region, control rods at region boundary, and 1.4224-cm (0.56-in.) lattice pitch[11].

[11] Fig. A-10, p. 46, Att. A, Ref. 1.

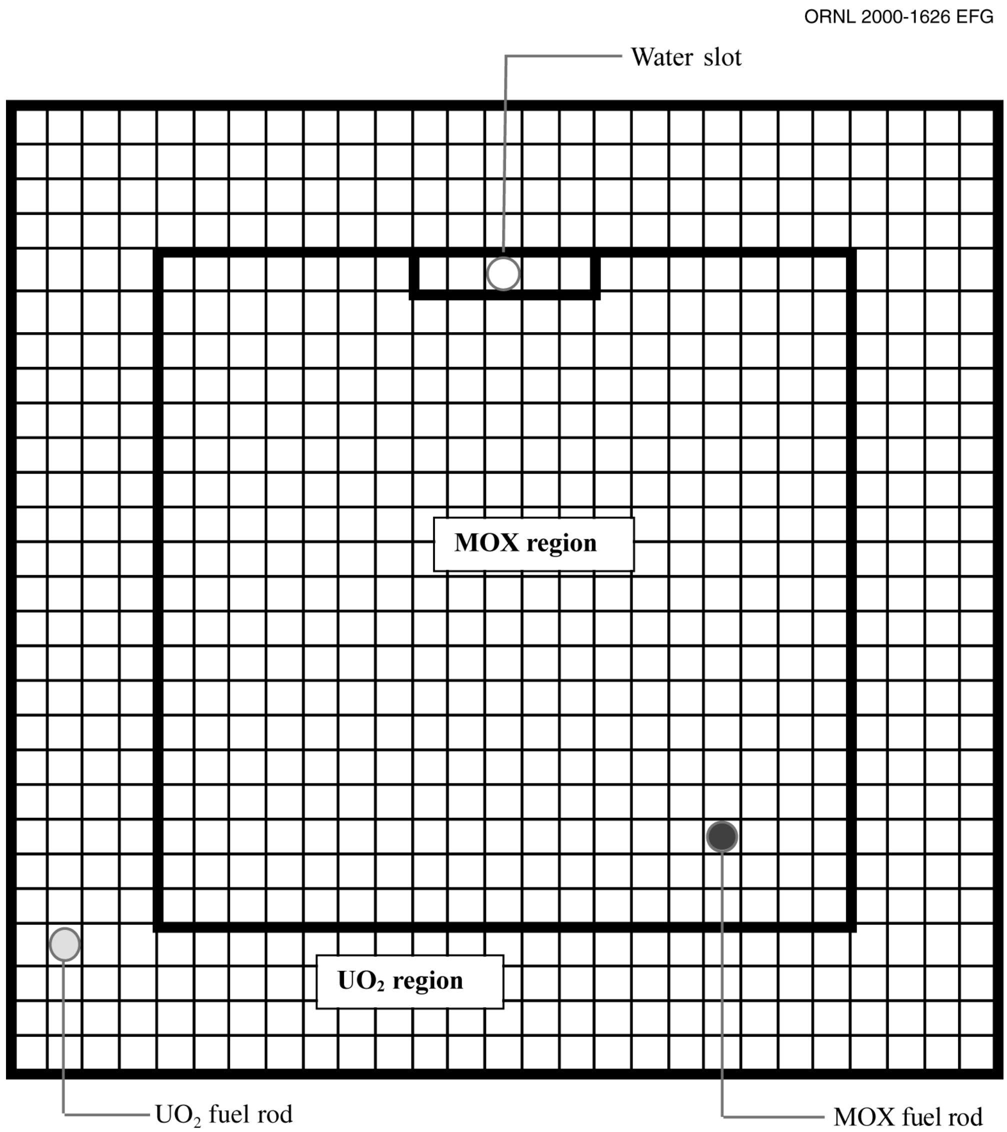

Figure 10. SX4.2.4: 27x27 core, 19x19 MOX center region, UO_2 outer region, water slot at boundary, and 1.4224-cm (0.56-in.) lattice pitch[12].

[12] Fig. A-11, p. 47, Att. A, Ref. 1.

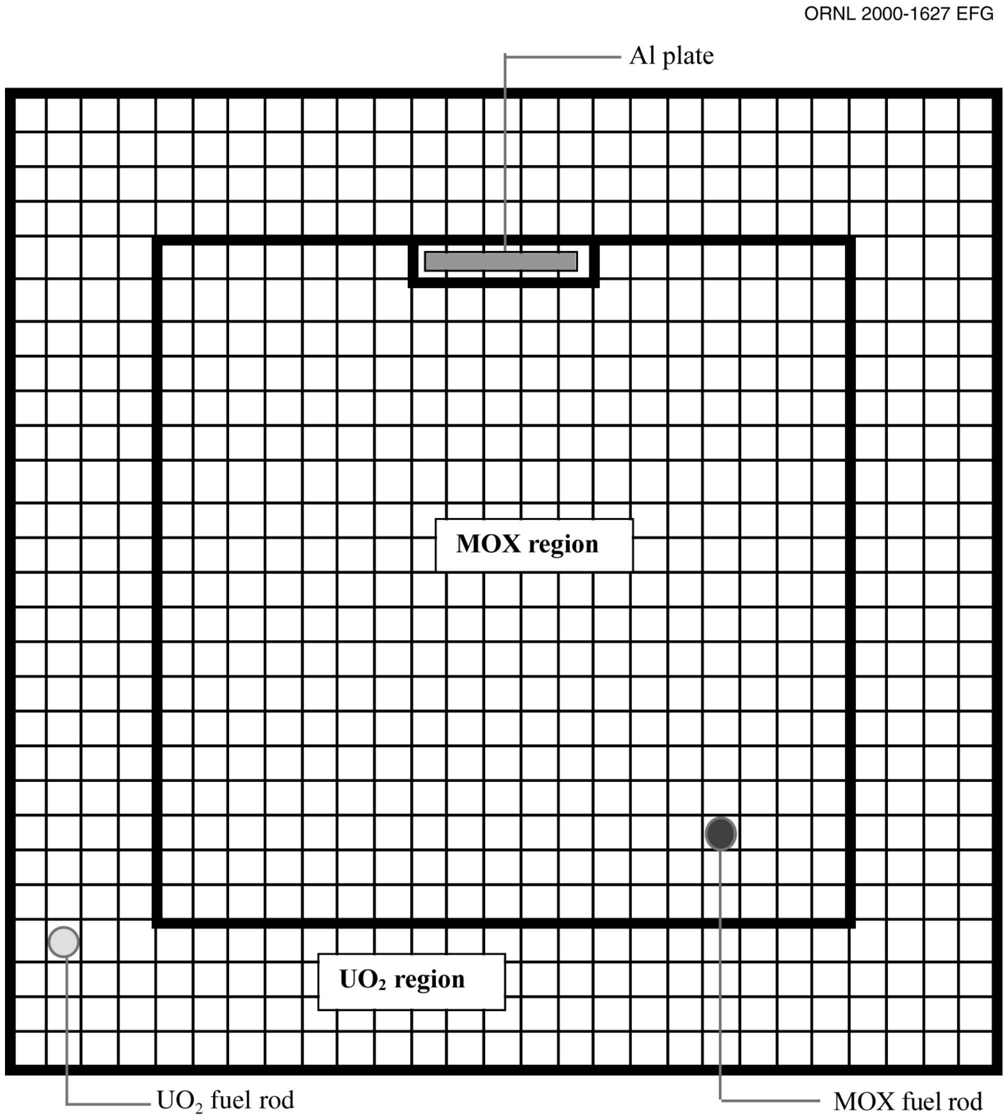

Figure 11. SX4.2.5: 27x27 core, 19x19 MOX center region, UO_2 outer region, Al plate at region boundary, and 1.4224-cm (0.56-in.) lattice pitch[13].

[13] Fig. A-12, p. 48, Att. A, Ref. 1.

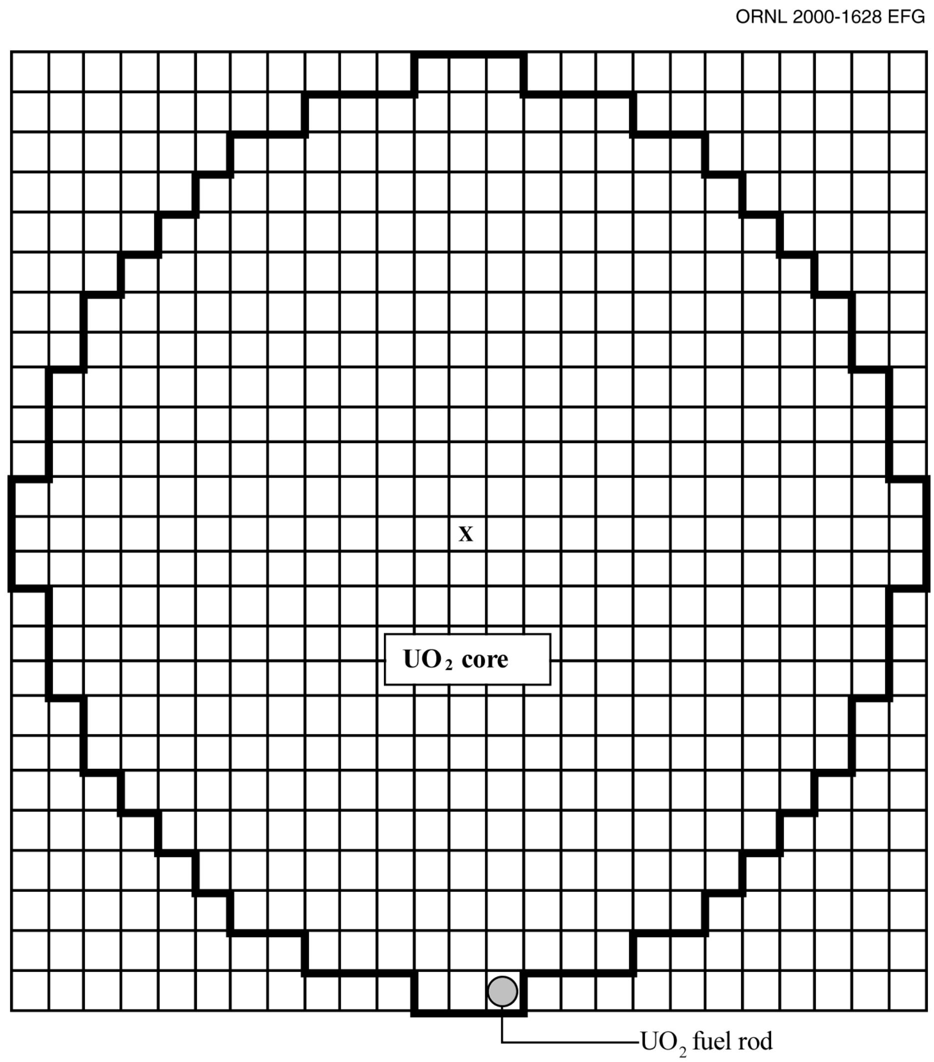

Figure 12. SX2.1.1: 449 UO_2 fuel rods, cylindrical core, and 1.3208-cm (0.52-in.) lattice pitch[14].

[14] Fig. B-10, p. 86, Ref. 1.

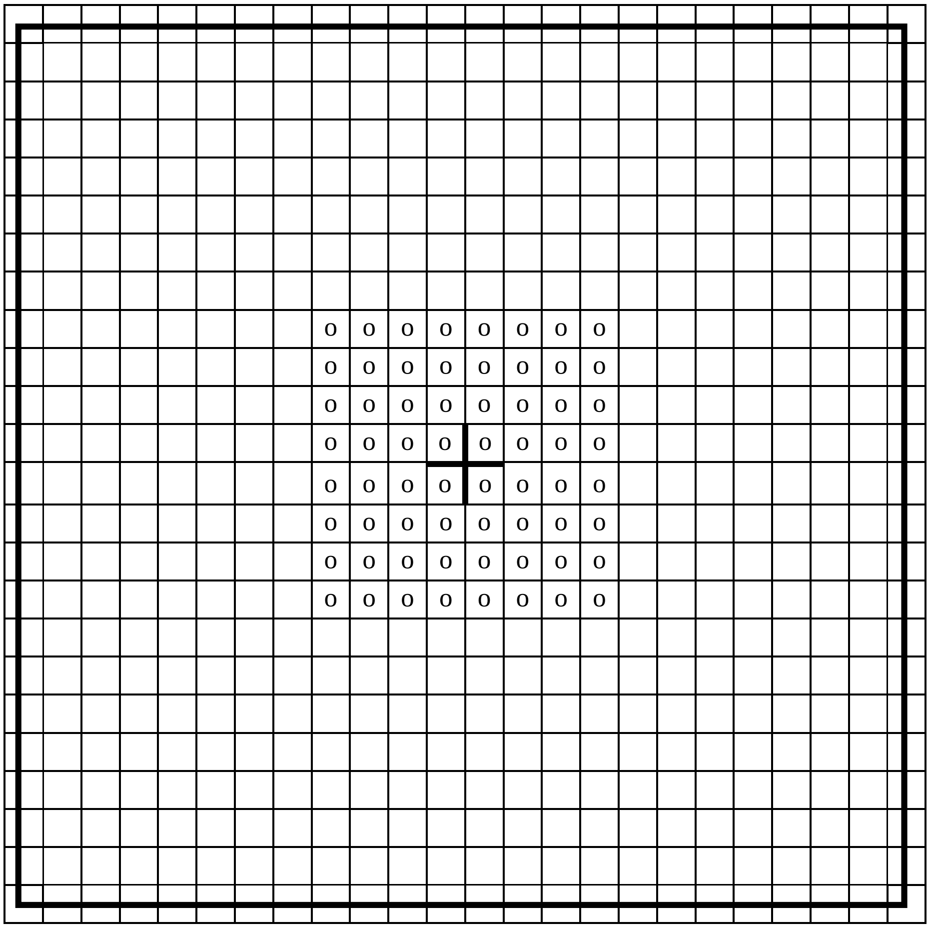

Figure 13. SX1.1.3: 23x23 MOX fuel rods, 8x8 voids, and 1.3208-cm (0.52-in.) lattice pitch[15].

[15] Fig. 3, p. 7, App. E, Ref. 1.

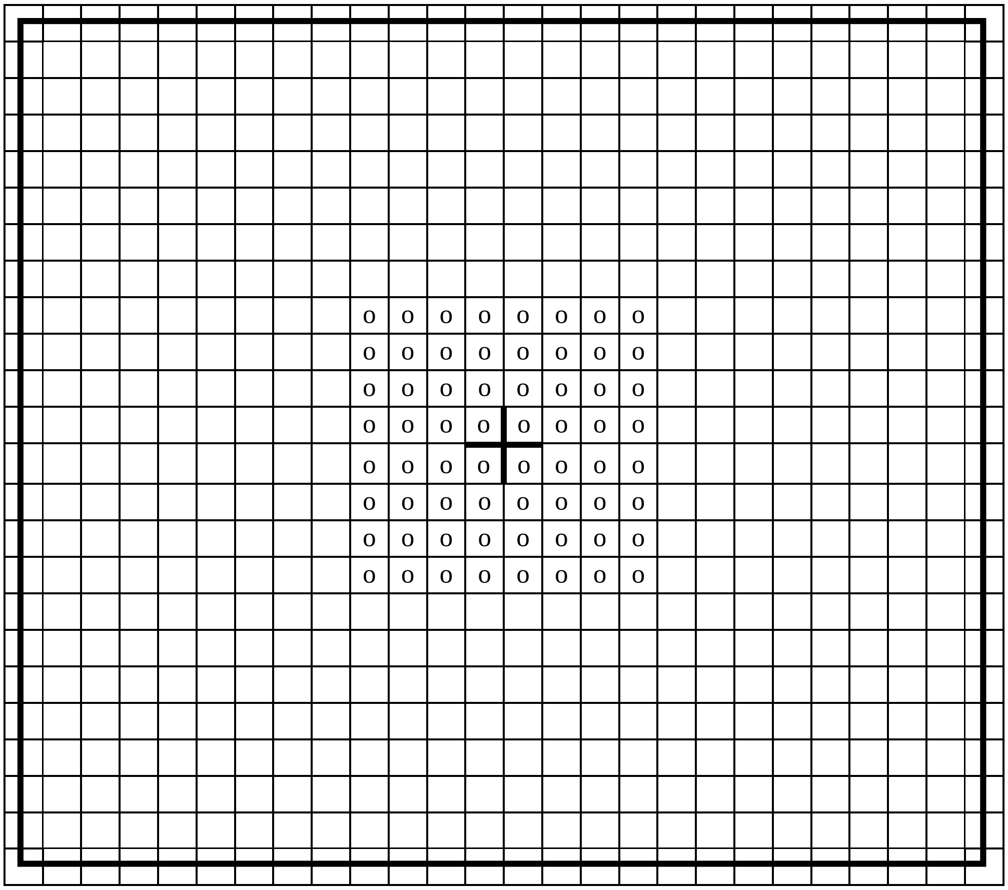

Figure 14. SX1.1.4: 25x23 MOX fuel rods, 8x8 voids, and 1.3208-cm (0.52-in.) lattice pitch[16].

[16] Fig. 4, p. 8, App. E, Ref. 1.

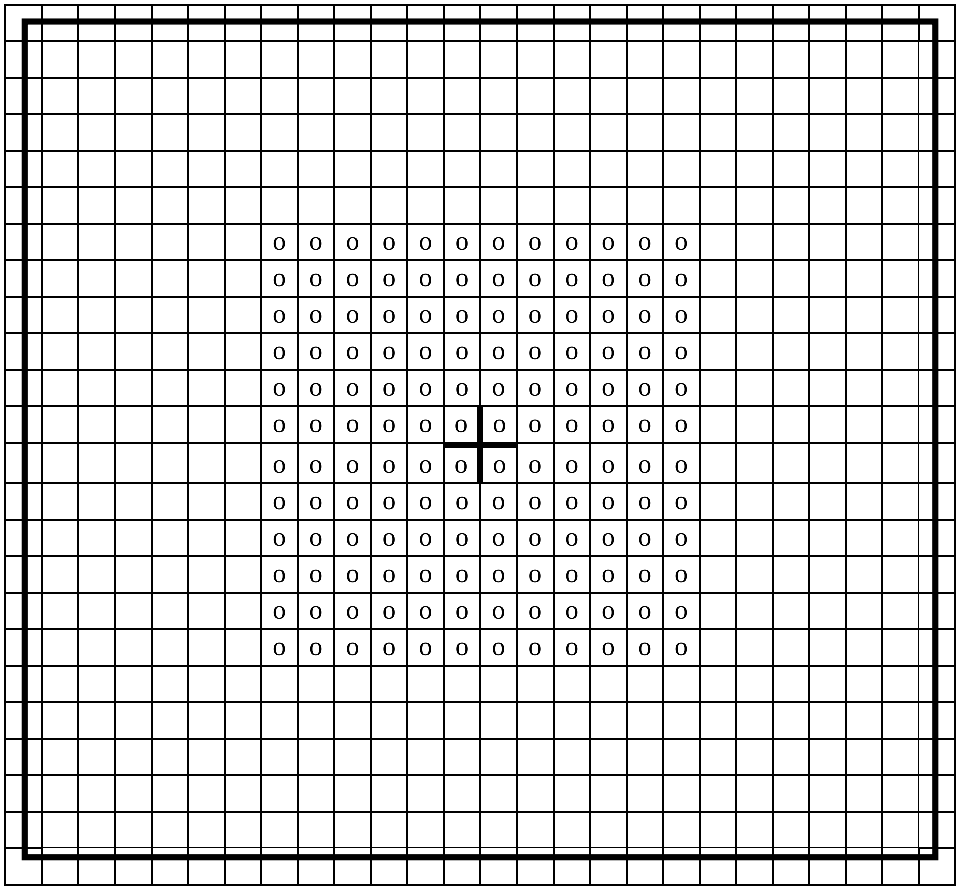

Figure 15. SX1.1.5: 25x23 MOX fuel rods, 12x12 voids, and 1.3208-cm (0.52-in.) lattice pitch[17].

[17] Fig. 5, p. 9, App. E, Ref. 1.

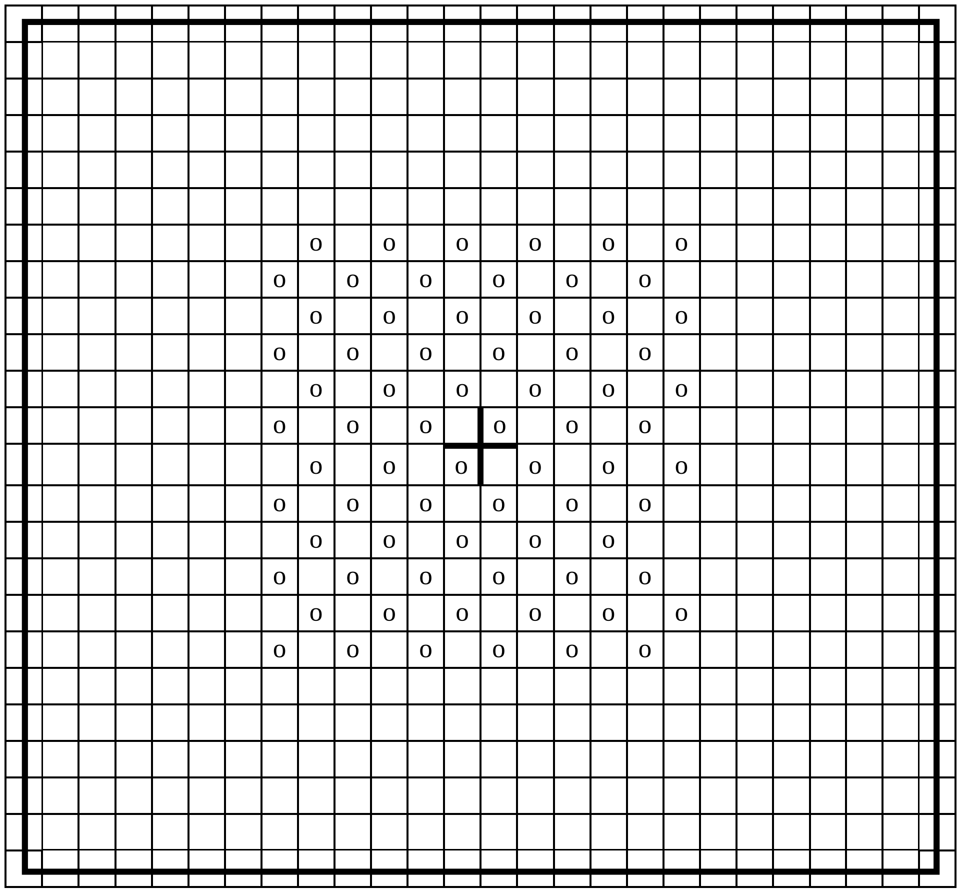

Figure 16. SX1.1.6: 25x23 MOX fuel rods, 72 voids, and 1.3208-cm (0.52-in.) lattice pitch[18].

[18] Fig. 6, p. 10, App. E, Ref. 1.

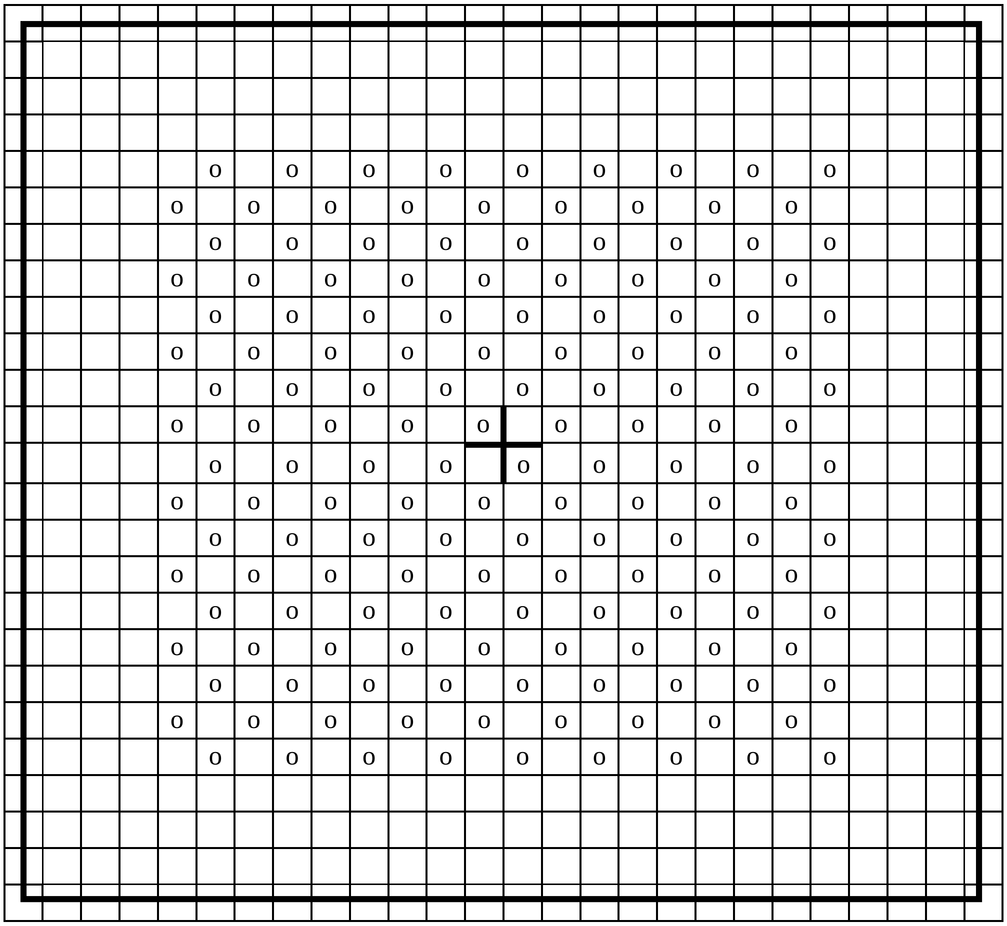

Figure 17. SX1.1.8: 25x24 MOX fuel rods, 153 voids, and 1.3208-cm (0.52-in.) lattice pitch[19].

[19] Fig. 8, p. 12, App. E, Ref. 1.

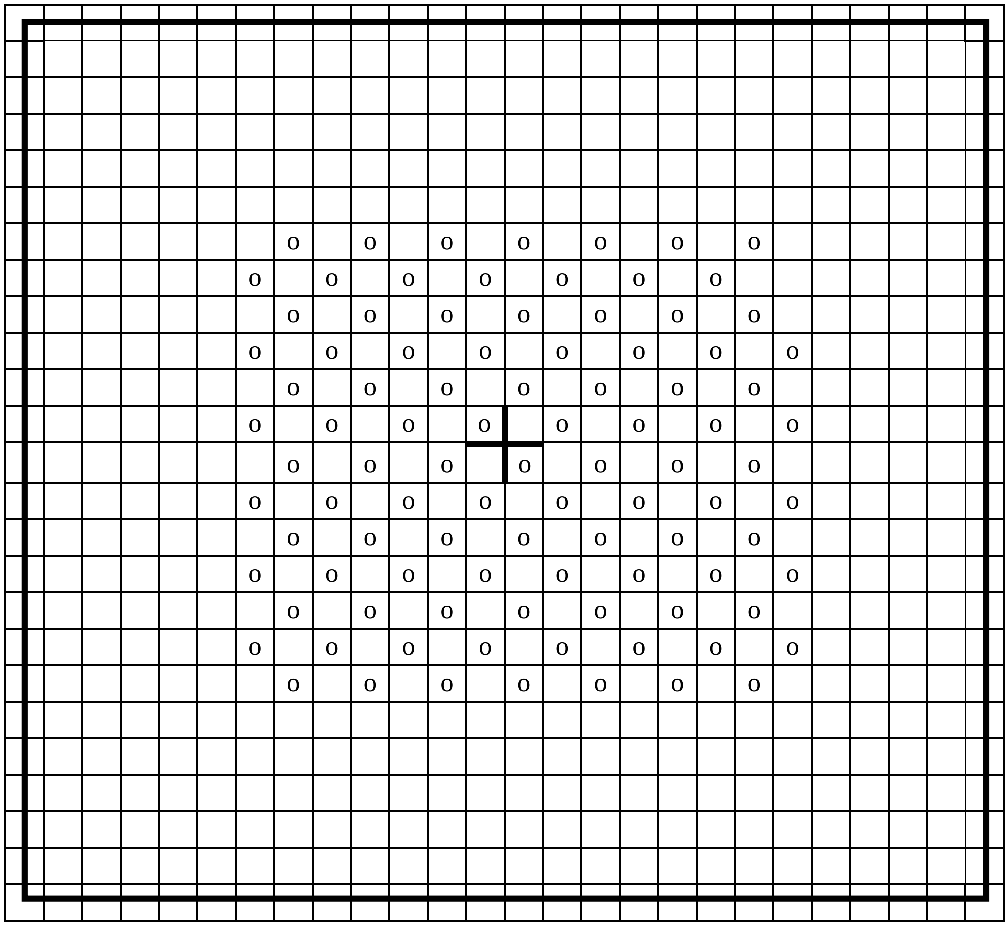

Figure 18. SX1.1.9: 25x24 MOX fuel rods, 91 voids, and 1.3208-cm (0.52-in.) lattice pitch[20].

[20] Fig. 9, p. 13, App. E, Ref. 1.

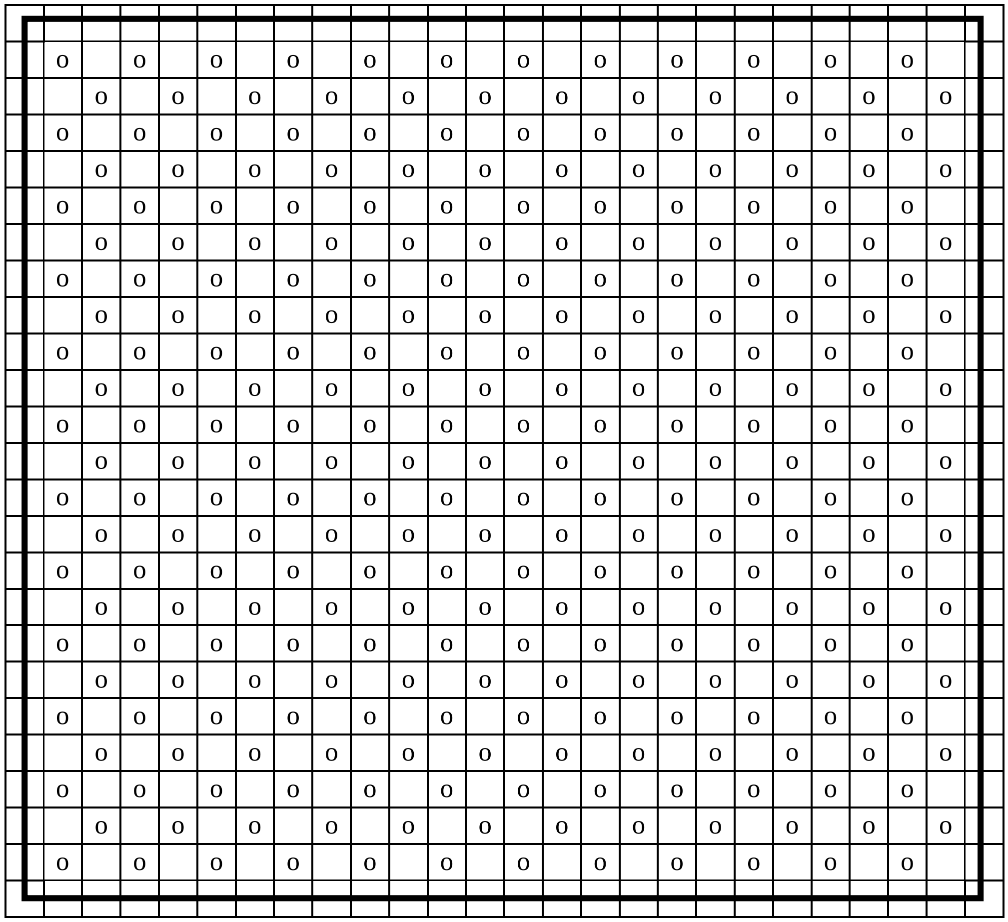

Figure 19. SX1.1.7: 25x24 MOX fuel rods, 276 voids, and 1.3208-cm (0.52-in.) lattice pitch[21].

[21] Fig. 7, p. 11, App. E, p. 11, Ref. 1.

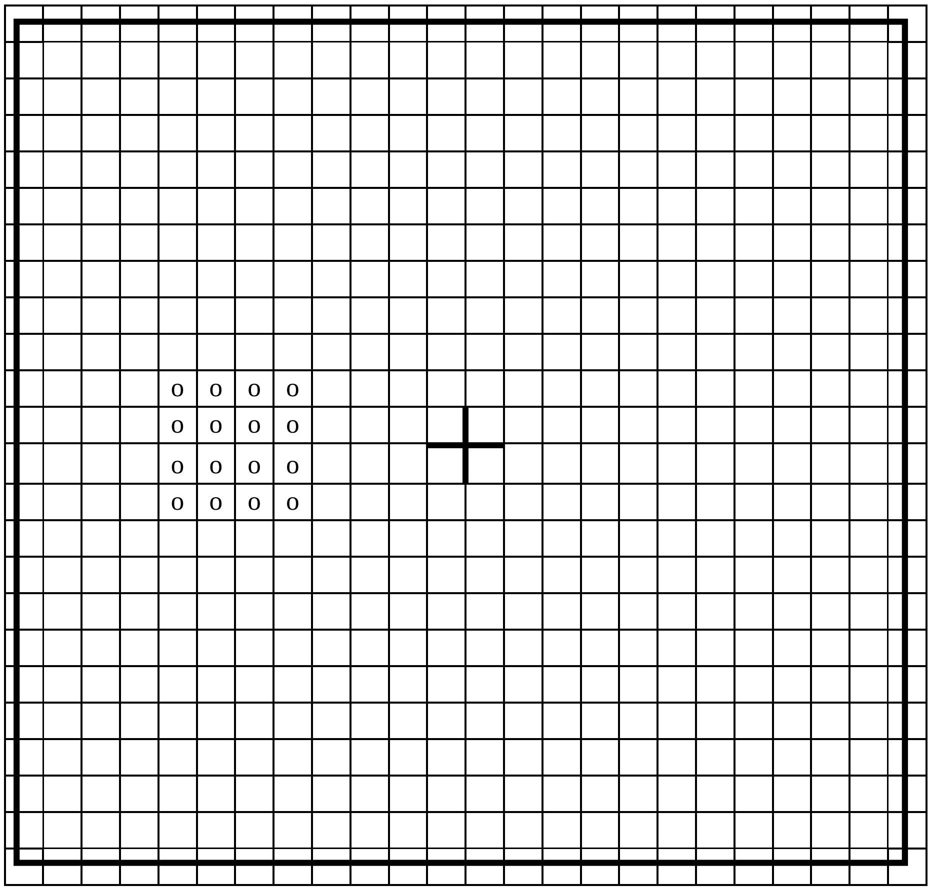

Figure 20. SX1.1.14[22]: 23x23 MOX fuel rods, 4x4 voids, and 1.3208-cm (0.52-in.) lattice pitch.

[22] The center of the 4x4 void array is displaced six fuel positions west relative to the center of the core (Fig. 14, p. 18, App. E, Ref. 1).

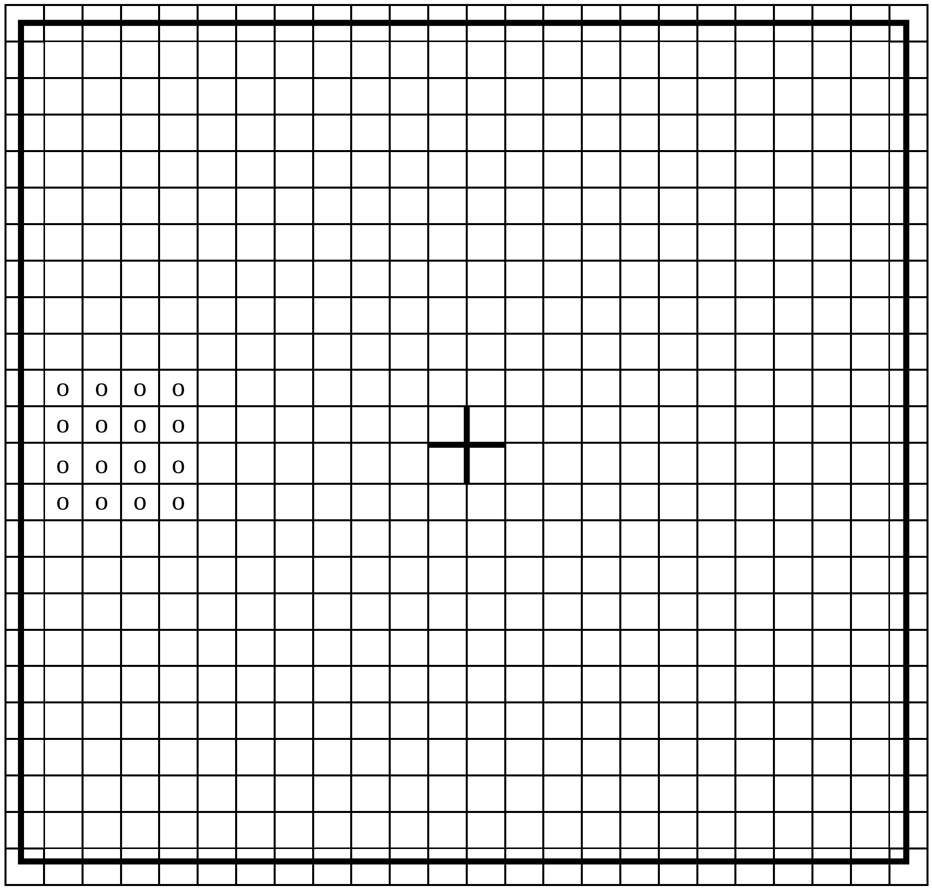

Figure 21. SX1.1.15[23]: 23x23 MOX fuel rods, 4x4 voids, and 1.3208-cm (0.52-in.) lattice pitch.

[23] The center of the 4x4 void array is displaced nine fuel rod positions west relative to the center of the core (Fig. 15, p. 19, App. E, Ref. 1).

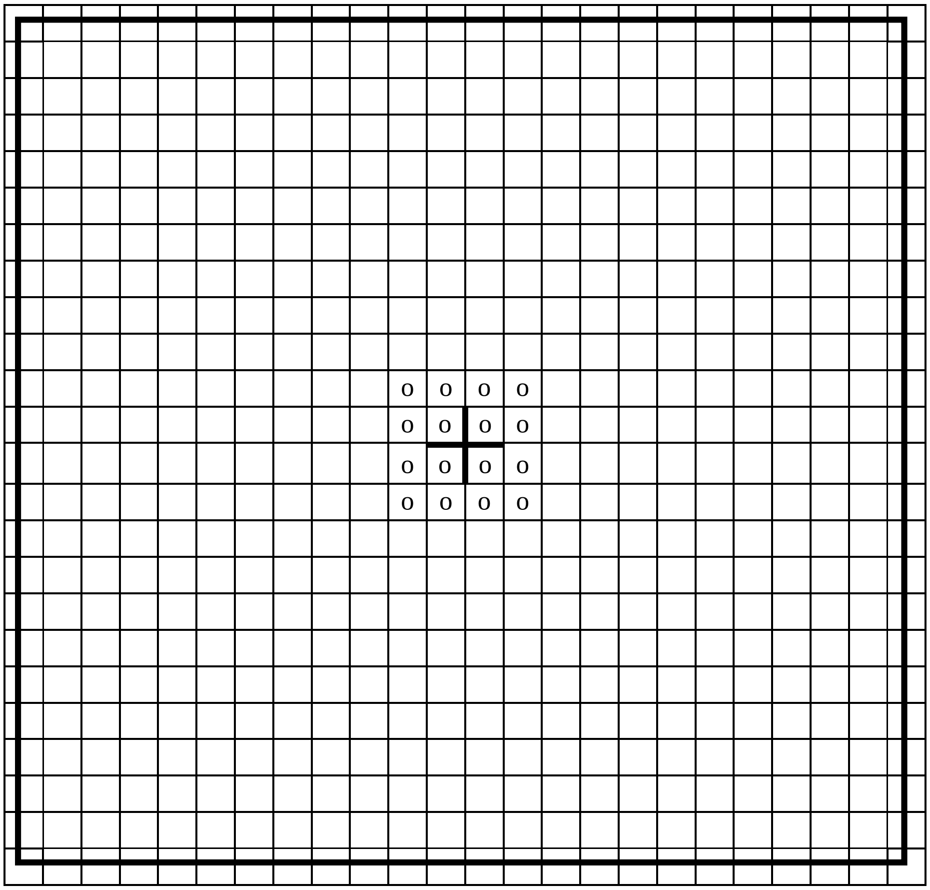

Figure 22. SX1.1.12: 23x23 MOX fuel rods, 4x4 voids, and 1.3208-cm (0.52-in.) lattice pitch[24].

[24] Fig. 12, p. 16, App. E, Ref. 1.

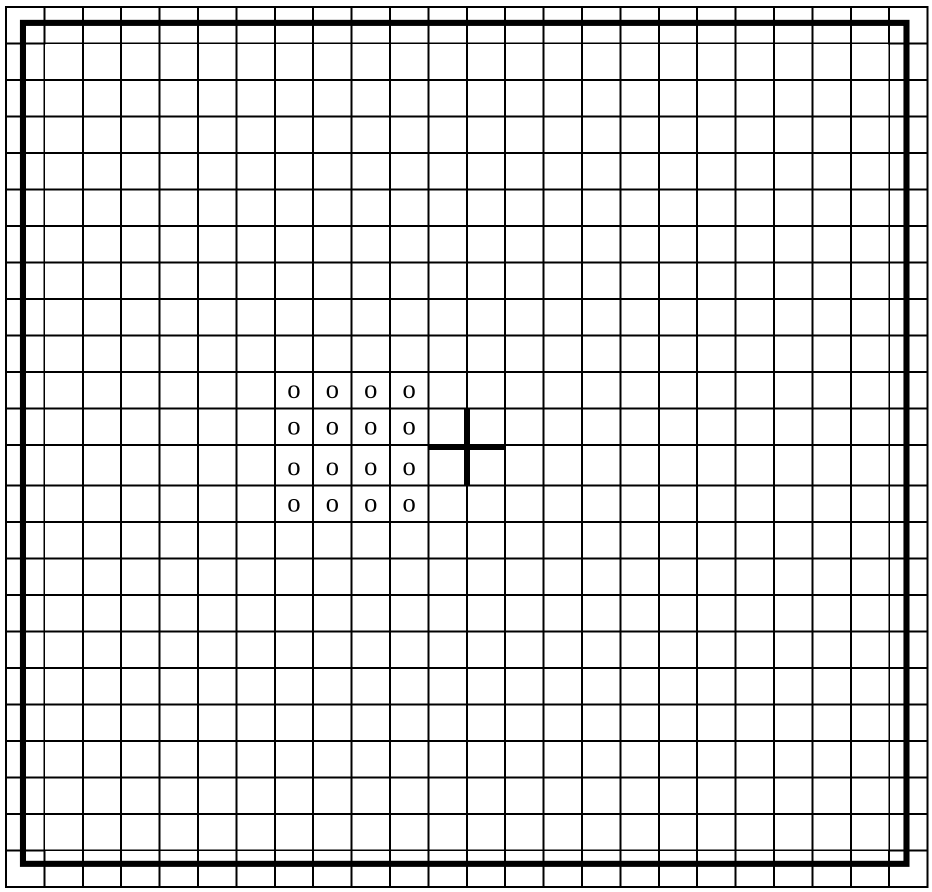

Figure 23. SX1.1.13[25]: 23x23 MOX fuel rods, 4x4 voids, and 1.3208-cm (0.52-in.) lattice pitch.

[25] The center of the 4x4 void array is displaced three fuel rod positions west relative to the center of the core (Fig. 13. p. 17, App. E, Ref. 1).

1.2.3 Description of the Fuel Pellets and the Fuel Rods

The MOX fuel used in the Saxton critical experiments was pelletized with a 0.857-cm (0.3374-in.) diameter and clad in Zircaloy-4 (Ref. 1, p. 42). Figure 24 shows the shape and ranges of dimensions of the fuel pellets, which were 0.92964 ± 0.0762-cm (0.366 ± 0.03-in.) long with a radius of 0.856996 ± 0.00254 cm (0.3374 ±0.001 in.), provided by Ref. 2, p. 41, Fig. 7C[26]. The pellets were dished at the bottom, which may account for some of the discrepancy between theoretical density and actual density of the fuel rod (see Evaluation of Experimental Data).

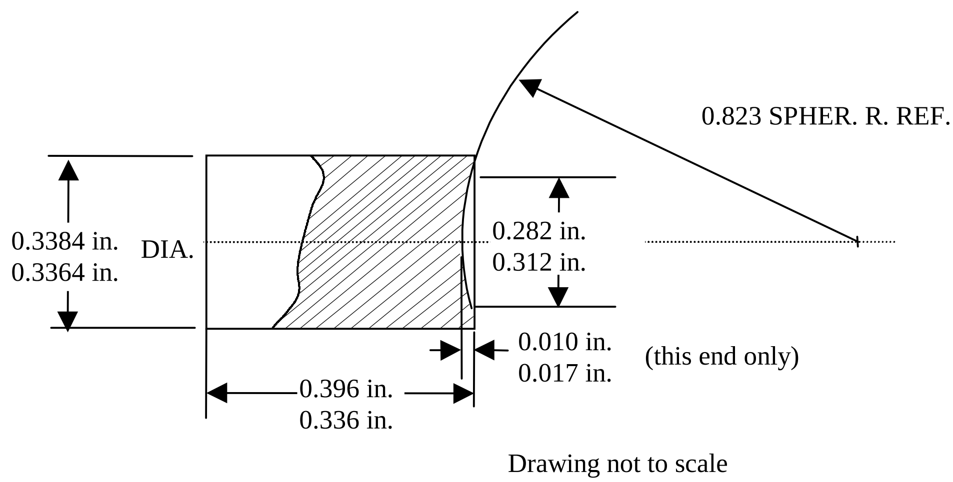

Figure 24. Fuel pellets schematics.

Figure 25 shows a schematic of the rods used in the critical experiments (Ref. 2, p. 39). The bottom part of the rod had, in ascending order, a welded end plug and one filler. The top part of the rod consisted, in a descending order, of a welded end plug, a predefined length for the spring, and fillers (at least one) in order to accommodate the pellet stack. Contrary to the Vipac fuel rods case, the blueprint does not predefine the length of the fuel stack. The fillers were made of Al_2O_3 (Ref. 2, p. 56).

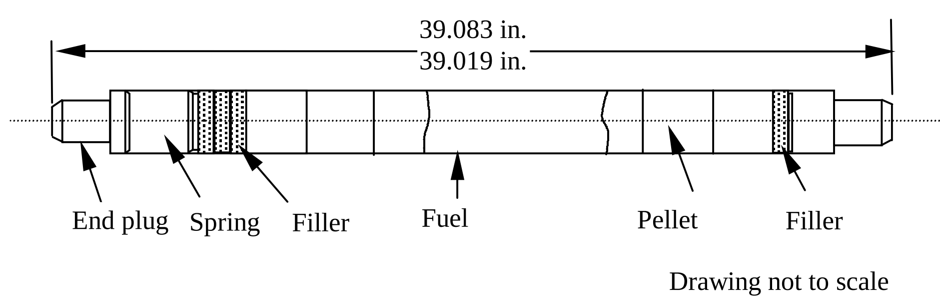

Figure 25. Fuel rod.

[26] Figure 7C, p. 41, Ref. 2 is titled "Saxton Plutonium Pellet Drawing for 304 SS Clading", which according to page 42, Ref. 1 should show a 0.90373-cm (0.3558-in.) diameter for the MOX pellet.

1.2.4 Description of the Assembly and Grid Structure

A typical core configuration is shown in Fig. 3. The fuel rods were inserted into a square pitch lattice through three aluminum plates (bottom, middle, and top guiding plates). The fuel rod holes were 1.00838 ± 0.00508 cm (0.397 ± 0.002 in.) in diameter. Water circulation in the core was enhanced by the presence of holes in the aluminum middle core grid. These water holes were 0.49022 ± 0.00254 cm (0.193 ± 0.001 in.) in diameter. The layout of these holes is shown in Fig. 26.

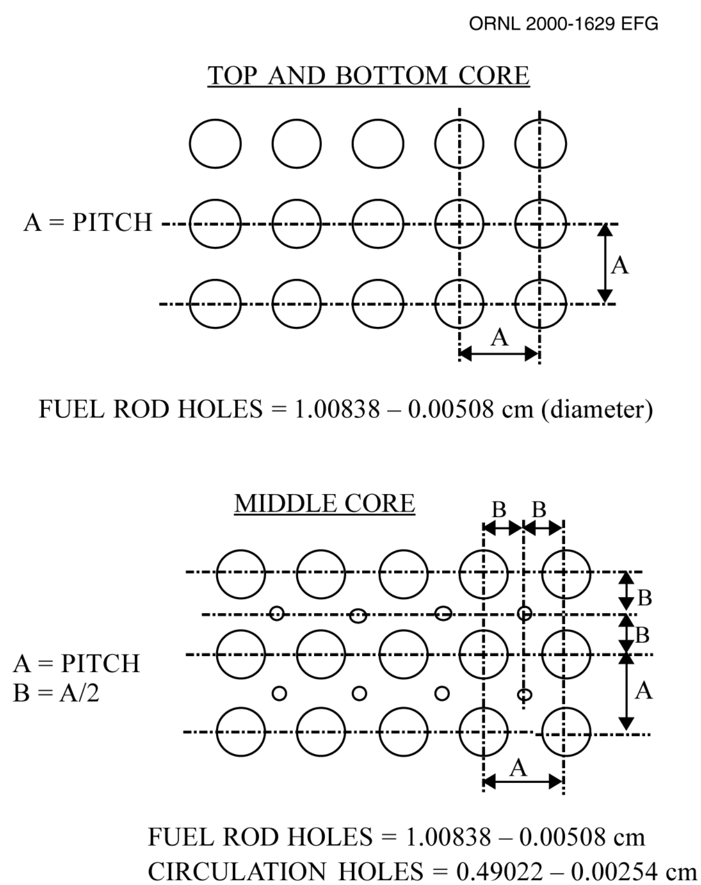

Figure 26. Layout of the holes in the top, bottom, and middle guiding plates.

As reported in the void-effect study (App. E, Ref. 1) each grid plate was a square 0.661 m × 0.661 m. The bottom grid structure rested on a 2.54-cm- (1-in.-) thick aluminum slab, the same size as the bottom grid. The 2.54-cm thick slab was itself supported by three 6.35-cm- (2-1/2-in.-) thick aluminum feet, which were placed on a 5.08-cm- (2-in.-) thick by 1.8288-m- (6-ft-) diameter aluminum slab/plate. This slab supported an approximately 1.8288 m (6-ft-) diameter tank that surrounded the grid structure and prevented water waves. Figures 27 (p.40, Att. A, Ref. 1) and 28 (p. 22, Ref. 1) give a description of the vertical cross section of the core. Note that the bottom of the active fuel appears at different heights above the bottom guide plate in the two figures.

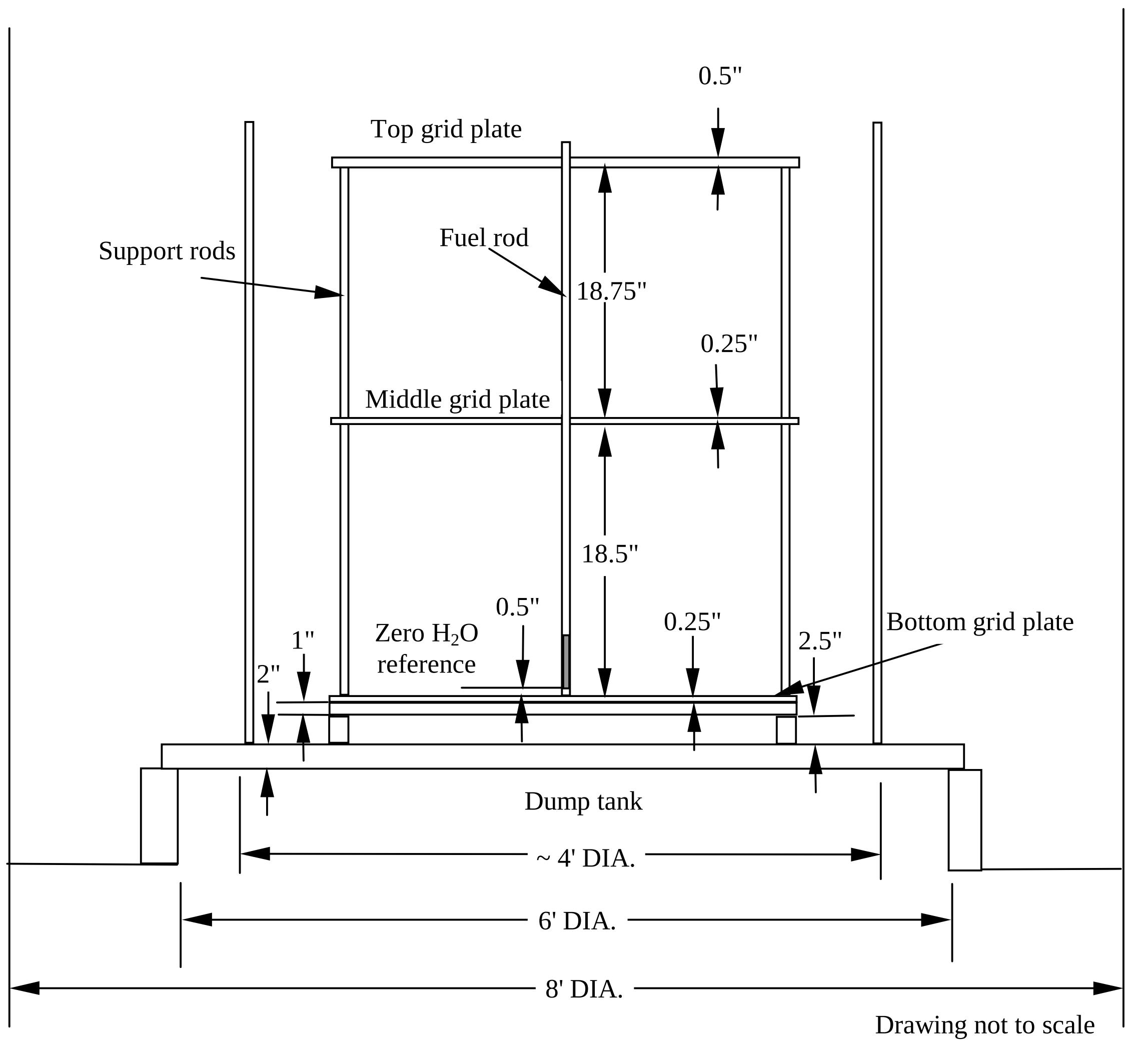

Figure 27. Cross section of the CRX core[27].

The top guide plate was 1.27-cm (0.5-in.) thick, while the center guide plate and the bottom plate were 0.635-cm (0.25-in.) thick. All guiding plates were aluminum. A typical fuel rod was 99.187-cm (39.05-in.) long and the bottom of the fuel started at 1.27 cm (0.5 in.) from the top of the bottom guide plate. The effective fuel length was 92.964 cm (36.6 in.). The center guide plate was 46.99 cm (18.5 in.) above the top of the bottom guiding plate. The top guiding plate was 47.625 cm (18.75 in.) above the top of the center guiding plate or 95.25 cm above the top of the bottom plate. According to Ref. 1, the guiding plates were supported by four 1.11125-cm (7/16-in.) diameter stainless steel (SS) support rods, which were covered by 1.5875-cm (5/8-in.) diameter aluminum pipe. The grid plates with their support rods made up the grid structure.

[27] "Zero H_2O reference" in this figure is the reference of the critical water heights reported in Ref. 1. However, Table 1.1 presents the corrected critical water heights, which are measured from the top of the core support plate.

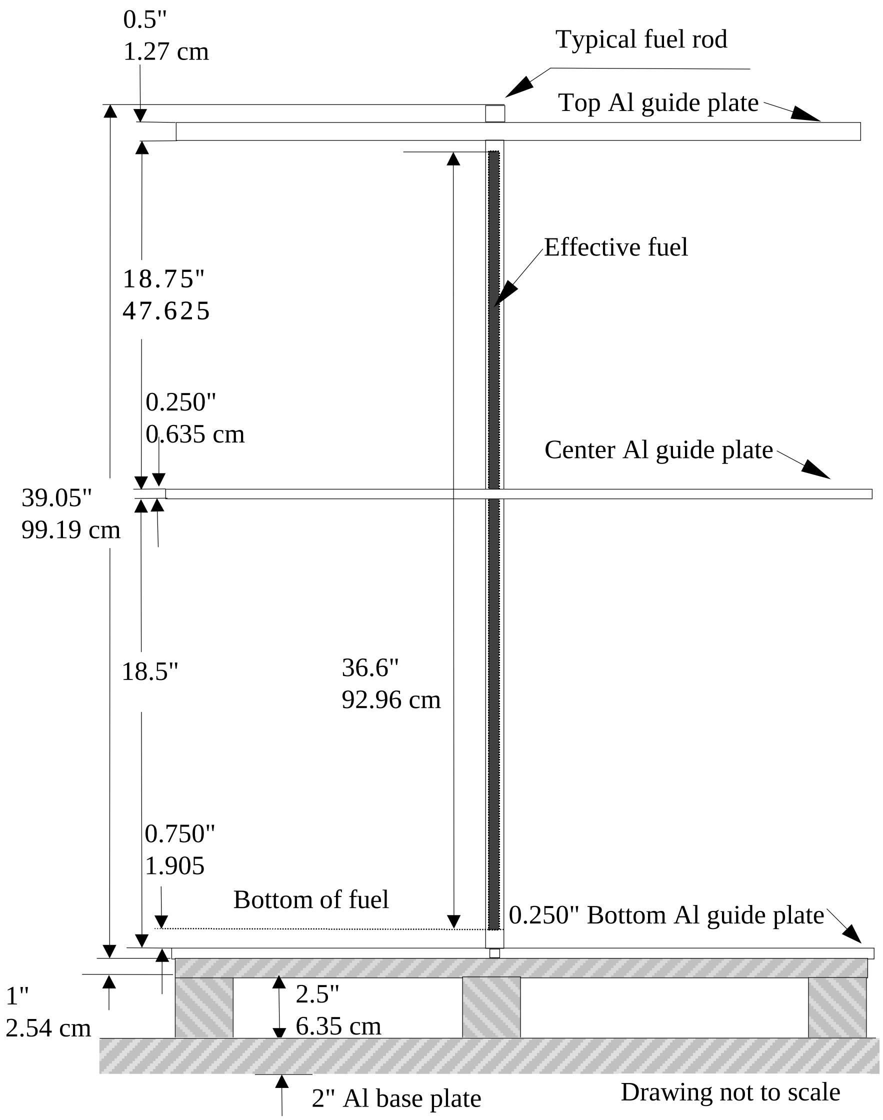

Figure 28. General cross section of the core.

1.2.5 Description of the Water Slot, Aluminum Plate, Control Rods, and Void Tubes

Different effects were investigated using a water slot, an aluminum plate, and control rods as described in Table 1.1. In the reactivity worth of perturbations to the uniform critical lattices of the single-region experiments, the water slot was formed by omitting five fuel rods from the center of a 19×19 core. The five remaining holes were in a line parallel to one side of the core with the third hole at the core center.

The aluminum plate was positioned between the guide plates in the space left by the five water holes described previously. Plate dimensions were 0.635-cm (0.25-in.) thick by 7.112-cm

(2.80-in.) wide. It is supposed that the Al plate filled the entire space between the core guiding plates on the vertical direction.

The control rods, composed of an unclad alloy[28] of 5% Cadmium, 15% Indium and 80% Silver [3], were 1.02362-cm (0.403-in.) in diameter. The control rods were inserted in the water slot described previously, and the size of the core was increased to 21×21 fuel rods. In the multiregion experiments, these perturbations were positioned at the interface of the two different fuel regions, as shown in Figures 8 through 11.

The aluminum void tubes were 1.45-m long, with the outer diameter of 0.4725 cm, and a wall thickness of 0.0127 cm. For the void-effect experiments, the core grid plates were fabricated with holes interstitial to the fuel rod positioning holes.

1.3 DESCRIPTION OF MATERIAL DATA

Fuel specifications are provided by Ref. 1, Att. A, p. 42. Two types of fuel rods were part of this experimental program. The first type was a low enriched uranium dioxide fuel rod, for which rod specifications are presented in Table 1.2.

Table 1.2. UO_2 rod specification

Weight percent of ^{235}U in UO_2	5.742
UO_2 weight	604.25 g
Weight fraction of U metal	0.8813
% theoretical density	93.0
Pellet diameter	0.90678 cm (0.357 in.)
Clad outer diameter	0.99314 cm (0.391 in.)
Clad inner diameter	0.91694 cm (0.361 in.)
Active fuel length	92.964 cm (36.6 in.)
Clad material	304 SS

The second fuel rod was made of mixed PuO_2 and UO_2. Uranium was natural enrichment. MOX rod specifications are presented in Table 1.3. The isotopic composition of the metal plutonium is given in Table 1.4.

[28] Reference 1 indicates the following element mass fraction for the control rods: 80% Cd, 15 % In, 5% Ag (App. A, p. 6). This high content of cadmium used in MCNP calculations led to an unacceptably small value for the effective multiplication factor. The results were similar to those obtained for the other critical configurations when using the element mass fractions provided in Ref. 10.

Table 1.3. MOX rod specification[29]

Weight percent of PuO_2	6.6
PuO_2-UO_2 weight	546.576 g
PuO_2 weight	36.074 g
Pu metal	31.815 g
% theoretical density[30]	94.0
Pellet diameter	0.856996 cm (0.3374 in.)
Clad outer diameter	0.99314 cm (0.391 in.)
Clad inner diameter	0.87503 cm (0.3445 in.)
Active fuel length	92.964 cm (36.6 in.)
Fuel rod length [2]	99.18954 cm (39.051 in.)
Clad material	Zircaloy 4

Table 1.4. Isotopic composition of the metal plutonium in the MOX fuel rod

Isotope	Weight[31] (g)	Weight Percent
^{239}Pu	28.789	90.50
^{240}Pu	2.727	8.57
^{241}Pu	0.283	0.89
^{242}Pu	0.013	0.04
	TOTAL	100.00

There is no specification for the type of aluminum used in this experiment. The assumption will be made that it is Al 6061. Table 1.5 lists the chemical composition of Al 6061 [4]. The density of this material is 2.7 g/cm^3.

[29] Also, the fabrication specifications SAX-P001 (Ref. 2, pp. 47 and 48) indicated the following reqirements: ratio of oxygen to metal in the plutonium-uranium pellet shall be between 1.97 and 2.02; the ratio of plutonium to uranium in any pellet sample shall be 0.071 ± 0.001; total plutonium plus uranium content shall be 87.8% by weight minimum; the total thermal macroscopic cross section imparted by rare earth and other impurities shall not exceed 100×10^{-5} cm^2/cm^3; and the pelletized MOX fuel blend shall be sufficiently homogeneous. Specifications SAX-P003, for fuel rod inspection and loading requirements for pelletized MOX fuel required that the weight of plutonium in any random 100 rods be controlled to ± 0.15% of the specified weight.

[30] The specification for the density of the pellets claded in Zircaloy was 94 ± 2 percent of the theoretical density (Ref. 2, pp. 6 and 41). The theoretical density shall be calculated by linear interpolation between the theoretical densities of UO_2 and PuO_2 (11.46 g/cm^3 and 10.96 g/cm^3, respectively).

[31] The weights of Pu isotopes sum to 31.812 g, which is smaller than the specified Pu metal weight (31.815 g).

Table 1.5. Aluminum 6061 chemical composition

Element	Wt. %
Mg	1.0
Al	96.7
Si	0.6
Ti	0.15
Cr	0.20
Mn	0.15
Fe	0.7
Cu	0.25
Zn	0.25

Tables 1.6 and 1.7 list the chemical components of 304 SS [5] and Zircaloy 4 [6], respectively. The density of stainless steel is 7.92 g/cm^3, and that of Zircaloy is 6.56 g/cm^3.

Table 1.6. Stainless steel 304 chemical composition

Element	Wt. %
Fe	69.5
Cr	19.0
Ni	9.5
Mn	2.00

Table 1.7. Zircaloy 4 chemical composition

Element	Wt. %
Zr	98.24
Fe	0.21
Sn	1.45
Cr	0.1

1.4 SUPPLEMENTAL EXPERIMENTAL MEASUREMENTS: RELATIVE POWER DISTRIBUTION

The evaluation of relative power and power sharing experiments is available in Ref. 7.

2. EVALUATION OF EXPERIMENTAL DATA

Two major inconsistencies are to be analyzed: a density mismatch for the MOX and UO_2 rods and the inconsistency regarding the position of the bottom of pellet stack from the bottom guide plate as shown in different figures.

2.1 DENSITY MISMATCH

The information provided by Ref. 1 for the density, the volume and the mass for each UO_2 and MOX rods are inconsistent with data found elsewhere. If one calculates the volume of the fuel through the use of the height of the fuel stack, and use 94% theoretical density, then one obtains a weight different from the specified rod weight. In Ref. 2, p. 79, the following statement about the plutonium loading can be read: "The weight of the plutonium in each pelletized rod was controlled by the plutonium assay of the batch and the pellet stack weight. The pellet stack was weighed before it was inserted into the tube. The tube content of each rod was calculated from the fuel weight and the Pu assay." In other words, this statement specifically indicates that the most reliable information is the total weight of the fuel and the plutonium concentration. As shown in Fig. 25, the length of the fuel stack was not a required dimension in the fabrication process. One filler at the bottom and at least one filler at the top were required. The blueprint [3] of the fuel stack states that approximately 100 fuel pellets will fit the rod, which is consistent with the dimension of the fuel stack, as given in Ref. 1 [100×0.92964 cm = 92.964 cm (36.6 in.)]. This information leads to an inconsistency regarding the reported density of the fuel. The average volume of the fuel stack is $V = 92.964\pi\,(0.856996)^2/4 = 53.624\ \text{cm}^3$ and the average density of the mixed oxide pellet, calculated by linear interpolation, is $\rho = (0.066 \times 0.94 \times 11.46 + (1\text{-}0.066) \times 0.94 \times 10.96) = 10.33342\ \text{g/cm}^3$. The resulting average rod weight is then 554.119 g, which exceeds the reported weighed, 546.576 g, by 7.543 g. Some possible scenarios account for this mass difference.

The first scenario relates the mass difference due to the dish end of each pellet. Ref. 2, p. 48 indicates the following formula may be used to calculate the average weight of fuel removed by dished ends: $(1/6)\pi\, h(3r^2+h^2)16.387D$, where h is the average dish height in inches, r is the average radius in inches, and D is the nominal density in g/cm^3. Using 10.33342 g/cm^3 for pellet densities and the corresponding values shown in Fig. 24 for the other parameters, a weight of 2.43 g is obtained, which is insufficient alone to account for the mass difference of 7.543 g.

The second scenario relates the mass difference to the maximum diameter allowed in the original purchase order [2]. The diameter dimension of the pellet can be as large as 0.859536 cm (0.3384 in.) If all the pellets in the rod had this dimension, the gain in mass would be 3.3 g per rod, which is still insufficient alone to account for the 7.5-g difference.

The last scenario considers the production density of the pellets, which should be 94 ± 2% of the theoretical density, according to the fabrication specifications. A density of 92.72% of the theoretical density for a homogenized effective fuel region within a radius of 0.4285 cm (0.1687 in.), and a length of 92.964 cm (36.6 in.) accounts for a mass of 546.576 g. The first two scenarios are not capable either alone or together to account for the discrepancy between the specified and actual fuel densities. A most likely answer resides in a combination of the three scenarios. Assuming the reported weights and effective fuel rod lengths correct for the two fuel types, the fuel densities of 10.19268 g/cm^3 for the homogenized MOX fuel and 10.06468 g/cm^3 for the homogenized UO_2 fuel are considered for benchmark calculations.

2.2 WATER REFERENCE INCONSISTENCY REPORTED IN FIGURES 27 and 28

Figure 27 shows the reference for the measured water moderator height, which was the bottom of the pellets stack, at 1.27 cm (0.5 in.) above the top of the bottom guide plate, while Fig. 28 presents the bottom of the fuel at 1.905 cm (0.75 in.) above the top of the bottom guide plate. This reporting translates respectively to a bottom of the fuel at 1.905 cm (0.75 in.) above the end of the fuel rod plug (or equivalently the bottom of the bottom guiding plate) in Fig. 27 and at 2.54 cm (1 in.) in the case of Fig. 28. On page 5, App. A, Ref. 1, note 4 states "one quarter in. thick aluminum grid plate at 45.7 cm from bottom of the fuel". According to Figures 27 and 28, there is a 46.99-cm (18.5-in.) distance between the bottom of the middle Al guide plate and the top of the bottom Al guide plate. If one subtracts 1.27 cm (0.5 in.) from 46.99 cm (18.5 in.), one obtains 45.72 cm (18 in.) between the bottom of the fuel and the bottom of the middle Al guide plate. This number is very close to the 45.7 cm mentioned in note 4. Therefore, 1.905 cm (0.75 in.) between the bottom of the fuel and the bottom of the bottom Al guide plate prevails over 1.27 cm (0.5 in.).

2.3 WATER HEIGHT

According to Ref. 1 (p. 26) "All water height data reported in all appendices were analyzed using relative difference only. For obtaining absolute water heights in relation to the bottom of the <u>fuel</u>, the following correction should be applied: $H_{corr} = 0.997 (H_{raw} + 1.91)$ cm".

According to the note 2 on page 5 of Ref. 1, the water heights listed were specifically referenced to the bottom of the fuel. If all the reported water heights are relative differences reported to the bottom of the fuel, then a correction for the absolute water heights must be applied. Therefore, we need to add to the reported water heights the distance from the zero-water reference to the top of the core support, which is 1.905 cm (0.75 in.). This leads to the following formula: $H_{corr} = H_{raw} + 1.905$ (cm), which is practically the same as the formula presented on page 26 of Ref. 1. Figure 27 and the statements on page 5 were prepared by the same author [1]. This statement is another compelling argument for considering that the position of the bottom of the fuel is 1.27 cm (0.5 in.), as indicated in Fig. 27, instead of 1.905 cm (0.75 in.), as indicated in Fig. 28, from the top of the bottom core plate. Table 1.1 contains the critical water height corrected according to the formula recommended on page 26 of Ref. 1.

2.4 MISSING DATA

The aluminum type for the guiding plates, the slab used in perturbation and power measurement experiments, and the tubes in the void-effect experiments is not provided by Ref. 1. Aluminum 6061 will be used in calculations[32].

The height of aluminum slab used in perturbation and power measurement experiments was not provided. It will be taken to be that of the core.

For control rods, only the outer diameter and the chemical composition were specified. Their height was chosen to be the same as that of the fuel rods. Also, the actual densities of the constituent elements will be used in the atomic density calculations for the control rod material.

Specifications for the end plug, fillers, and spring are missing. The fillers and spring will be neglected and their corresponding volumes will be filled by Zircaloy 4.

[32] MCNP perturbation calculations for a material change from Al 6061 to ^{27}Al indicated insignificant differences in k_{eff}. Thus, Δk_{eff} were 1.5359E-04, 4.5886E-05, 6.1569E-05, 3.5930E-05, and 9.4497E-5 for cores SX1.1.1, SX1.2.1, SX1.3.1, SX1.4.1, and SX1.5.1, respectively.

3. BENCHMARK SPECIFICATIONS

3.1 DESCRIPTION OF THE MODEL

The core configuration is shown in Fig. 27[33]. The fuel rods are inserted in a square pitched lattice through three aluminum guiding plates (top, middle and bottom guiding plates), as shown in Figs. 2 and 3. The layout of the holes in Al guide plates is shown in Fig. 26. The core size, pattern, fuel type, moderator temperature and critical height measured from the bottom of the bottom Al guide plate, and the boron concentration for each critical experiment are presented in Table 1.1. The reflector at the bottom of the core is water and at the top of the core is air and fuel rods. The specified masses for MOX and UO_2 active fuel regions are homogenized within the specified fuel rod radii and lengths.

3.2 DIMENSIONS

The top guide plate is 1.27-cm thick, while the center and the bottom guiding plates are 0.635-cm thick. The center guide plate is 46.99 cm above the top of the bottom guiding plate. Its dimensions are 66.1 cm $\times$ 66.1 cm. The top guiding plate is 47.625 cm above the top of the center guide plate or 95.25 cm above the top of the bottom plate. The fuel rod holes are 1.00837 cm (tolerance is 0.00508 cm) in diameter. Water circulation in the core was enhanced by the presence of holes in the aluminum middle core grid. These water holes are 0.49022 cm (tolerance is 2.54E-3 cm) in diameter. The bottom grid structure rests on a 2.54-cm-thick aluminum slab, the same size as the bottom grid. The 2.54-cm-thick slab is itself supported by 6.35-cm thick aluminum feet, which stand on a 5.08 cm thick by 1.8288 m in diameter aluminum slab/plate. This slab supports a tank approximately 1.2192 m in diameter, which surrounds the grid structure and prevents water waves. The guiding plates are supported by four 1.1125-cm SS support rods, which are covered with 1.5875-cm-diameter aluminum pipe. All the components of core grid structure are assumed to be made from Al 6061, for which Table 3.5 gives element atomic densities.

The MOX fuel rod consists of the active fuel region, which is a cylinder of 0.856996 ± 0.0762 -cm diameter and 92.964-cm height, and a Zircaloy 4 clad of 0.87503-cm inner diameter and 0.99314-cm outer diameter. The fuel rod height is 99.18954 ± 0.08128 cm. The atomic densities for the active fuel region and clad are provided in Tables 3.2 and 3.3, respectively.

The UO_2 fuel rod consists of the active fuel region, which is a cylinder of 0.90678-cm diameter and 92.964-cm height, and the 304 SS clad of 0.91694-cm inner diameter and 0.99314-cm outer diameter. The fuel rod height is also 99.18954 cm. The atomic densities for the active fuel region and clad are provided in Tables 3.1 and 3.4, respectively.

The aluminum slab used in some experiments (see core description in Table 1.1) has the dimensions of 0.635-cm thick by 7.112-cm wide. It is assumed that the slab height is the same

---

[33] Reference 4 is an evaluation of seven critical experiments involving different lattice pitches, identified as MIX-COMP-THERM-003. Although limited in scope, the benchmark specifications presented by this reference for general core description are applicable to most of the critical experiments evaluated in the present document.

as the core height. The control rods, with a 1.02362-cm diameter, are composed of an unclad alloy of 5% Cadmium, 15% Indium and 80% Silver. Table 3.6 presents element atomic densities for the control rods. The aluminum void tubes used in void-effect experiments are 1.45 m long, with the outer diameter of 0.4725 cm. The wall thickness of the tube is 0.0127 cm.

Table 3.7 presents the atomic densities for borated water used in some critical experiments, as shown in Table 1.1.

3.3 MATERIAL DATA

The atomic densities presented in this section were calculated according to the recommendations provided by Ref. 5. Reference 9 provided the element/isotope atomic masses.

Tables 3.1 and 3.2 list the atomic densities of the two fuel types components.

Table 3.1. Atomic densities for the UO_2 rod

Isotope/element	Atomic density (b^{-1}, cm^{-1})
^{235}U	1.3049E-3
^{238}U	2.1151E-2
O	4.4967E-2
Total	6.7422E-2

Table 3.2. Atomic densities for the MOX rod[34]

Isotope/element	Atomic density (b^{-1}, cm^{-1})
^{239}Pu	1.3524E-3
^{240}Pu	1.2755E-4
^{241}Pu	1.3193E-5
^{242}Pu	5.8920E-7
^{234}U	1.1677E-6
^{235}U	1.5286E-4
^{238}U	2.1077E-2
O	4.5453E-2
Total	6.8177E-2

Tables 3.3 through 3.7 list the atomic densities for the core structure plates; fuel clads, and control rods.

[34]These benchmark specifications are entirely within fabrication specifications. Thus, the ratio of oxygen to metal is 2.0002, the ratio of Pu to U is 0.0712, and the total Pu plus U content is 88.2% by weight (see Section 1.3).

Table 3.3. Zircaloy 4 atomic densities

Element	Atomic density (b^{-1}, cm^{-1})
Zr	4.2543E-2
Fe	1.4855E-4
Sn	4.8253E-4
Cr	7.5976E-5
Total	4.3250E-2

Table 3.4. 304 SS atomic densities

Element	Atomic density (b^{-1}, cm^{-1})
Fe	5.9356E-2
Cr	1.7428E-2
Ni	7.7197E-3
Mn	1.7363E-3
Total	8.6240E-2

Table 3.5. Al 6061 atomic densities

Element	Atomic density (b^{-1}, cm^{-1})
Mg	6.6897E-4
Al	5.8273E-2
Si	3.4736E-4
Ti	5.0952E-5
Cr	6.2541E-5
Mn	4.4394E-5
Fe	2.0381E-4
Cu	6.3967E-5
Zn	6.2163E-5
Total	5.9777E-2

Table 3.6. Ag-In-Cd alloy atomic densities[35]

Element	Atomic density (b^{-1}, cm^{-1})
Ag	4.3562E-2
In	7.6735E-3
Cd	2.6126E-3
Total	5.3849E-2

[35] The element densities are provided by Ref. 8, pp. M8.2.15 and M8.2.16.

The atomic densities for boron at different concentrations in water moderator are presented in Table 3.7. The natural atomic abundances of B10 and B11 considered for these calculations were 19.9% and 80.1%, respectively up to 2% higher ^{10}B concentration has been observed in some natural boron samples, i.e., 20.3% ^{10}B.

Table 3.7. Boron concentration and atomic densities

Boron concentration (ppm)	Moderator Temperature (^0C)	Atomic density (b^{-1}, cm^{-1})			
		B-10	B-11	O	H
25	16.9	2.7681E-07	1.1142E-06	3.3391E-02	6.6777E-02
50	16.9	5.5365E-07	2.2285E-06	3.3392E-02	6.6776E-02
228	18	2.5254E-06	1.0165E-05	3.3398E-02	6.6757E-02
309	18	3.4233E-06	1.3779E-05	3.3403E-02	6.6755E-02
337	18	3.7345E-06	1.5032E-05	3.3412E-02	6.6767E-02
1252	20	1.3901E-05	5.5954E-05	3.3454E-02	6.6699E-02
1425	18.5	1.5834E-05	6.3734E-05	3.3476E-02	6.6713E-02
1453	17.8	1.6149E-05	6.5000E-05	3.3482E-02	6.6721E-02
1453	18	1.6148E-05	6.4998E-05	3.3481E-02	6.6718E-02
1453	18.2	1.6147E-05	6.4995E-05	3.3479E-02	6.6716E-02

3.4 TEMPERATURE DATA

Experimental temperature data for each case is listed in Table 1.1.

3.5 EXPERIMENTAL AND BENCHMARK-MODEL K_{EFF}

The k_{eff} for each case was 1.000 except for the following cases:

SX2.4.1: k_{eff} = 1.00156
SX4.2.5: reactor period is +140 seconds

4. RESULTS OF SAMPLE CALCULATIONS

Table 4.1 presents the results of criticality calculations performed with MCNP-4B [10] and the continuous cross section libraries processed from the evaluated nuclear data files ENDF/B-V and ENDF/B-VI, which are listed in Table 4.2. The S(alpha, beta) table for hydrogen in light water at 300K was also used in all cases.

Table 4.1. Calculated Effective Multiplication Factors, K_{eff}[36]

	$K_{eff} \pm \sigma$	
Core designation	MCNP-4B/ENDF/B-V	MCNP-4B/ENDF/B-VI
SX1.1.1[37]	0.9972 ± 0.0005	0.9915 ± 0.0005
SX1.2.2	0.9995 ± 0.0003	0.9936 ± 0.0003
SX1.2.3	0.9990 ± 0.0003	0.9929 ± 0.0003
SX1.2.4	0.9984 ± 0.0003	0.9927 ± 0.0003
SX1.2.5	0.9990 ± 0.0003	0.9927 ± 0.0003
SX1.2.7	0.9988 ± 0.0005	0.9925 ± 0.0005
SX1.2.8	0.9971 ± 0.0005	0.9912 ± 0.0005
SX1.2.9	1.0005 ± 0.0005	0.9941 ± 0.0005
SX1.2.10	0.9976 ± 0.0005	0.9921 ± 0.0005
SX1.2.11	0.9980 ± 0.0005	0.9924 ± 0.0005
SX1.2.12	0.9997 ± 0.0005	0.9930 ± 0.0005
SX1.3.1	1.0041 ± 0.0005	0.9964 ± 0.0005
SX1.4.1	1.0057 ± 0.0005	0.9977 ± 0.0005
SX1.5.1	1.0071 ± 0.0005	0.9997 ± 0.0005
SX2.2.1[38]	0.9967 ± 0.0005	0.9931 ± 0.0005
SX2.2.3	0.9965 ± 0.0005	0.9928 ± 0.0005
SX2.2.4	0.9974 ± 0.0005	0.9929 ± 0.0005
SX2.2.5	1.0005 ± 0.0005	0.9963 ± 0.0005
SX2.2.6	0.9957 ± 0.0005	0.9935 ± 0.0005
SX2.4.1	0.9986 ± 0.0005	0.9941 ± 0.0006
SX3.2.1	0.9968 ± 0.0003	0.9926 ± 0.0003
SX3.2.2	0.9991 ± 0.0003	0.9934 ± 0.0003
SX3.2.3	0.9981 ± 0.0003	0.9933 ± 0.0003
SX3.2.4	0.9976 ± 0.0003	0.9934 ± 0.0003
SX4.2.1	0.9990 ± 0.0003	0.9952 ± 0.0003
SX4.2.2	0.9998 ± 0.0003	0.9940 ± 0.0003
SX4.2.3	0.9995 ± 0.0003	0.9952 ± 0.0003
SX4.2.4	0.9994 ± 0.0003	0.9950 ± 0.0003

[36] The computer operating system used for MCNP calculations is UNIX.
[37] Cores SX1.2.1, SX1.2.2, and SX1.2.6 had the same configuration (see Table 1.1).
[38] Cores SX2.2.1 and SX2.2.2 had the same configuration (see Table 1.1).

Core designation	$K_{eff} \pm \sigma$	
	MCNP-4B/ENDF/B-V	MCNP-4B/ENDF/B-VI
SX4.2.5	1.0011 ± 0.0003	0.9954 ± 0.0003
SX5.2.1	0.9984 ± 0.0003	0.9933 ± 0.0003
SX6.2.1	0.9960 ± 0.0003	0.9930 ± 0.0003
SX1.1.2	0.9992 ± 0.0005	0.9920 ± 0.0005
SX1.1.3	0.9985 ± 0.0005	0.9906 ± 0.0005
SX1.1.4	1.0010 ± 0.0005	0.9930 ± 0.0005
SX1.1.5	0.9982 ± 0.0005	0.9928 ± 0.0005
SX1.1.6	0.9986 ± 0.0005	0.9926 ± 0.0005
SX1.1.7	0.9971 ± 0.0005	0.9926 ± 0.0005
SX1.1.8	0.9979 ± 0.0005	0.9922 ± 0.0005
SX1.1.9	0.9989 ± 0.0005	0.9919 ± 0.0005
SX1.1.10	1.0018 ± 0.0005	0.9931 ± 0.0005
SX1.1.12	0.9975 ± 0.0005	0.9919 ± 0.0005
SX1.1.13	0.9975 ± 0.0005	0.9917 ± 0.0005
SX1.1.14	0.9975 ± 0.0005	0.9918 ± 0.0005
SX1.1.15	0.9977 ± 0.0005	0.9920 ± 0.0005

Table 4.2. Cross section library tables used in criticality calculations

ENDF/B-V			ENDF/B-VI		
ZAID[39]	Library name	Source	ZAID	Library name	Source
1001.50c	Rmccs	B-V.0	1001.60c	Endf60	B-VI.1
5010.50c	Rmccs	B-V.0	5010.60c	Endf60	B-VI.1
5011.50c	endf5p	B-V.0	5011.60c	endf60	B-VI.0
7014.50c	Rmccs	B-V.0	7014.60c	endf60	B-VI.0
8016.50c	Rmccs	B-V.0	8016.60c	endf60	B-VI.0
12000.50c	endf5u	B-V.0	12000.60c	endf60	B-VI.0
13027.50c	Rmccs	B-V.0	13027.60c	endf60	B-VI.0
14000.50c	endf5p	B-V.0	14000.60c	endf60	B-VI.0
22000.50c	endf5u	B-V.0	22000.60c	endf60	B-VI.0
24000.50c	Rmccs	B-V.0	24050.60c	endf60	B-VI.1
			24052.60c	endf60	B-VI.1
			24053.60c	endf60	B-VI.1
			24054.60c	endf60	B-VI.1
25055.50c	endf5u	B-V.0	25055.60c	endf60	B-VI.0
26000.50c	endf5p	B-V.0	26054.60c	endf60	B-VI.1
			26056.60c	endf60	B-VI.1
			26057.60c	endf60	B-VI.1
			26058.60c	endf60	B-VI.1

[39] Nuclide identifier in MCNP.

ENDF/B-V			ENDF/B-VI		
ZAID[39]	Library name	Source	ZAID	Library name	Source
28000.50c	Rmccs	B-V.0	28000.50c	endf5p	B-V.0
29000.50c	Rmccs	B-V.0	29063.60c	endf60	B-VI.2
			29065.60c	endf60	B-VI.2
40000.60c	endf60	B-VI.1	40000.60c	endf60	B-VI.1
47000.55c	Rmccsa	T-2	47107.60c	endf60	B-VI.0
			47109.60c	endf60	B-VI.0
48000.50c	enfd5u	B-V.0	48000.50c	endf5u	B-V.0
49000.60c	endf60	B-VI.0	49000.60c	endf60	B-VI.0
92234.50c	endf5p	B-V.0	92234.60c	endf60	B-VI.0
92235.50c	Rmccs	B-V.0	92235.60c	endf60	B-VI.2
92238.50c	Rmccs	B-V.0	92238.60c	endf60	B-VI.2
94240.50c	Rmccs	B-V.0	94240.60c	endf60	B-VI.2
94241.50c	endf5p	B-V.0	94241.60c	endf60	B-VI.1
94242.50c	endf5p	B-V.0	94242.60c	endf60	B-VI.0

REFERENCES

1. E. G. Taylor, “Saxton Plutonium Program: Critical Experiments for the Saxton Partial Plutonium Core,” EURAEC-1493, WCAP-3385-54, Westinghouse Electric Corporation (December 1965).

2. A. Bancheria, R. N. Stanutz, R. J. Allio, M. D. Houston, W. E. Ray, R. C. Rose, “Saxton Plutonium Program: Material Design and Fabrication of the Saxton Partial Plutonium Core,” EURAEC-1492, WCAP-3385-53, Westinghouse Electric Corporation (December 1965).

3. W. R. Smalley, D. B. Scott, “Metallurgical Evaluation of Silver-Indium-Cadmium Control Rods Alloys,” WCAP-3269-29, Westinghouse Electric Corporation (August 1964).

4. American Society for Metals (ASM) International Handbook Committee, *Aluminum and Aluminum Alloys,* ASM International (1994).

5. C. D. Harmon, II, R. D. Busch, J. F. Briesmeister, R. A. Foster, “Criticality Calculations with MCNP: A Primer,” LA-12827-M, Los Alamos National Laboratory (LANL) (August 1994).

6. J. P. Frick, *Woldman’s Engineering Alloys: Material Data Series,* 7th Edition, ASM International (1990).

7. C. Radulescu, N. M. Abdurrahman, M. L. Adams, “Evaluation of Relative Power Experiments for the Saxton Partial Plutonium Core,” ORNL/SUB/99-XSZ175V-7, Oak Ridge National Laboratory (ORNL) (to be published).

8. L. M. Petrie, P. B. Fox, K. Lucius, “Standard Composition Library,” ORNL/NUREG/CSD-2/V3/R6, ORNL (September 1998).

9. *Nuclides and Isotopes, Fifteenth Edition,* General Electric Company (1996).

10. J. F. Briesmeister, “MCNP-A General Monte Carlo N-Particle Transport Code,” LA12625-M, Version B, LANL (1997).

INTERNAL DISTRIBUTION

1–5. B. B. Bevard
6. J. J. Carbajo
7. E. D. Collins
8. B. S. Cowell
9. M. D. DeHart
10. F. C. Difilippo
11. R. J. Ellis
12–16. J. C. Gehin
17. S. R. Greene
18. T. W. Horning
19. D. T. Ingersoll
20. H. T. Kerr
21. M. A. Kuliasha
22. G. E. Michaels
23. C. V. Parks
24. D. L. Moses
25–29. R. T. Primm III
30. C. C. Southmayd
31. ORNL Central Research Library
32–33. ORNL Laboratory Records (OSTI)
34. ORNL Laboratory Records-RC

EXTERNAL DISTRIBUTION

35. N. Abdurrahman, College of Engineering, Dept. of Mechanical Engineering, University of Texas, Austin, TX 78712
36. M. L. Adams, Department of Nuclear Engineering, Texas A&M University, Zachry 129, College Station, TX 77843
37. H. Akkurt, 2919 Cooley Building, 2355 Bonisteel Boulevard, Ann Arbor, MI 48109-2104
38. D. Alberstein, Los Alamos National Laboratory, MS-K551, P.O. Box 1663, Los Alamos, NM 87545
39. Dr. Kiyonori Aratani; Surplus Weapons Plutonium Disposition Group; International Cooperation and Nuclear Material Control Division; Japan Nuclear Cycle Development Institute; 4-49 Muramatsu, Tokai-rnura, Naka-gun, Ibaraki-ken, Japan
40. J. Baker, Office of Fissile Materials Disposition, U.S. Department of Energy, NN-63, 1000 Independence Avenue SW, Washington, DC 20585
41. J. B. Briggs, Idaho National Environmental and Engineering Laboratory, P.O. Box 1625-3855, Idaho Falls, ID 83415-3855
42. A. Caponiti, Office of Fissile Materials Disposition, U.S. Department of Energy, NN-63, 1000 Independence Avenue SW, Washington, DC 20585
43. M. S. Chatterton, Office of Nuclear Reactor Regulation, MS O10B3, United States Nuclear Regulatory Commission, Washington, DC 20555-0001
44. K. Chidester, Los Alamos National Laboratory, MS-E502, P.O. Box 1663, Los Alamos, NM 87545
45. Mr. Richard H. Clark, Duke/Cogema/Stone & Webster, 400 South Tryon Street, WC-32G, P.O. Box 1004, Charlotte, NC 28202
46. W. Danker, U.S. Department of Energy, NN-62, 1000 Independence Avenue SW, Washington, DC 20585

47. N. Fletcher, Office of Fissile Materials Disposition, U.S. Department of Energy, NN-63, 1000 Independence Avenue SW, Washington, DC 20585
48. T. Gould, Lawrence Livermore National Laboratory, P.O. Box 808, MS-L186, Livermore, CA 94551
49. L. Holgate, Office of Fissile Materials Disposition, U.S. Department of Energy, NN-60, 1000 Independence Avenue SW, Washington, DC 20585
50. L. Jardine, Lawrence Livermore National Laboratory, P.O. Box 808, MS-L166, Livermore, CA 94551
51. Dr. Alexander Kalashnikov, Institute of Physics and Power Engineering, 1 Bondarenko Square, Obninsk, Kaluga Region, Russia 249020

52–56. D. E. Klein, Associate Vice Chancellor for Special Engineering Programs, The University of Texas System, 210 West Sixth Street, Austin, TX 78701

57. Richard W. Lee, Office of Nuclear Reactor Regulation, MS O10B3, United States Nuclear Regulatory Commission, Washington, DC 20555-0001
58. Mr. Steve Nesbit, Duke/Cogema/Stone & Webster, 400 South Tryon Street, WC-32G, P.O. Box 1004, Charlotte, NC 28202
59. J. O. Nulton, Office of Fissile Materials Disposition, U.S. Department of Energy, NN-61, 1000 Independence Avenue SW, Washington, DC 20585
60. Nagao Ogawa; Director and General Manager; Plant Engineering Department; Nuclear Power Engineering Corporation; Shuwa-Kamiyacho Building, 2F; 3-13, 4-Chome Toranomon; Minato-Ku, Tokyo 105-0001, Japan
61. Dr. Stephen L. Passman, Booz-Allen & Hamilton, 555 13th Street, NW, No. 480E, Washington, DC 20004

62–66. Dr. Alexander Pavlovitchev, Russian Research Center “Kurchatov Institute,” Institute of Nuclear Reactors, VVER Division, VVER Physics Department, 123182, Kurchatov Square, 1, Moscow, Russia

67. K. L. Peddicord, Associate Vice Chancellor, Texas A&M University, 120 Zachry, College Station, TX 77843-3133
68. G. Radulescu, Framatome Cogema Fuels, 1261 Town Center Drive, MS-423, Las Vegas, NV 89143
69. W. D. Reece, Texas A&M University, Department of Nuclear Engineering, Zachry 129, College Station, TX 77843-3133
70. P. T. Rhoads, Office of Fissile Materials Disposition, U.S. Department of Energy, NN-61, 1000 Independence Avenue SW, Washington, DC 20585
71. E. Siskin, Office of Fissile Materials Disposition, U.S. Department of Energy, NN-60, 1000 Independence Avenue SW, Washington, DC 20585
72. U. Shoop, Office of Nuclear Reactor Regulation, MS O10B3, U.S. Nuclear Regulatory Commission, Washington, DC 20555-0001
73. J. Thompson, Office of Fissile Materials Disposition, U.S. Department of Energy, NN-61, 1000 Independence Avenue SW, Washington, DC 20585
74. F. Trumble, Westinghouse Savannah River Company, Building 730R, Room 3402, Aiken, SC 29808